Interferometric measurement of rotationally symmetric aspheric surfaces

Article *in* Proceedings of SPIE - The International Society for Optical Engineering · June 2009

DOI: 10.1117/12.830655

CITATIONS
43

READS
125

1 author:

Michael Kuechel
Utsunomiya University
31 PUBLICATIONS **264** CITATIONS

SEE PROFILE

Interferometric measurement of rotationally symmetric aspheric surfaces

Michael F. Küchel
Zygo Corporation, Laurel Brook Rd., Middlefield, CT 06455

ABSTRACT

The measurement of aspheric surfaces in a Fizeau interferometer implies a sometimes dramatic increase in dynamic range, in terms of acceptable slope and departure, which can run the risk of introducing substantial measurement errors. Common approaches to relaxing the dynamic range requirement include reducing the area of the surface measured in a single measurement and stitching together the partial results, or using compensation techniques with the help of additional components like null-lenses or computer generated holograms. This paper reviews these methods, with special attention to the questions of degrees of freedom for misalignment. These considerations lead to a proposed method that uses the inherent symmetry of the problem to scan along the optical axis, gathering measurements at zones of normal incidence. These measurements are independent from each other; their ensemble represents directly the surface-deviation in normal direction to the surface and the result is in the object coordinates of the design surface. Using an absolutely calibrated spherical reference surface, the result is absolute. It is shown that this is very different from the technique of stitching of zones, even when Intrinsic Coma is preserved through partially overlapping measurement regions.

Keywords: Aspheric surfaces, interferometric measurement, absolute measurement, scanning, stitching, Fizeau interferometer, Computer Generated Hologram, retrace errors, distortion, error analysis.

1. INTRODUCTION

Aspheric optical surfaces have been well known for a long time, and the problem of their measurement is almost a classical one. The reasons for using aspheres instead of spheres are to reach the necessary performance already with a lower number of lenses, and in many cases, where size and weight are restricted, aspheres act as enablers for the system altogether. [1,2] New, deterministic manufacturing methods, optics for consumer electronics, aerospace and defense applications as well as the revival of photography and cinematography through the development of digital sensors have led to a real breakthrough for the use of aspheres in optical systems. Today, one to three rotationally symmetric aspheric surfaces are used in nearly every new zoom lens that is released for digital SLR camera systems, the smaller lens-systems in point and shoot cameras as well as camera-phones contain aspheres, the pick-ups of DVD and blue-ray players are aspheric lenses, telescopes use aspheric mirrors and high-sophisticated lens-, mirror-, or catadioptric systems used for lithographic machines are not possible without a high percentage of aspheric surfaces. As mass production of molded lenses becomes more and more cost effective, and the difference in cost for a molded asphere compared to a sphere becomes relatively small, aspheric system solutions are becoming even cheaper. As a consequence, there is also a growing number of double sided, molded aspheres, which pose even higher demands on manufacturing and measurement.

As a consequence, the measurement of the aspheric surfaces during production has become an important challenge in the field of testing of optical surfaces. The general requirements are a consequence of constrains that are posed by the market onto the manufacturing department, which can be described by 3 key-phrases: *short time to market*, s*table quality*, and *cost down*. Different methods have been proposed [3,4,5,6,7,8,9,10,11,12,13,14,15,16,17,18] or are in use for in-house production [19,20,21,22,23,24,25,26,27,28,29,30,31] and some are developed to the point that they can be offered as a product. [32,33,34,35,36,37,38,39,40,41,42,43] For the assessment of these developments, many different characteristics must be taken into account, like the completeness and evidence of a measurement result for the part under test, largest aspheric departure that can be measured, allowed amount of deviation from the design surface, the possible dimensions of the parts (diameter, numerical aperture), measurement uncertainty and traceability of the result, and last but not least, spatial resolution. Other important factors to be considered are the cost for the measurement tool, ease of use, the time required for one complete measurement as well as touch time for the operator, the cost and lead-time for the tools to be manufactured before a measurement can be performed and requirements for space and temperature stability.

In this paper, we will mainly explain one solution that Zygo has taken to measure aspheric surfaces, but also some alternative approaches. We do not try to do this with any depth in engineering details, but in contrast, restrict ourselves to deal with their basic characteristics and compare and contrast from the standpoint of good metrology. It is clear that even this attempt is somehow subjective and might be controversial, and we might not always have the necessary insight in some details that influence the strength of an approach. But there are a number of guidelines or "rules of thumb" that a metrologist might use when searching for a solution. Finally, with brute force attempts, nearly all is possible today, but the elegance is, when a solution is simple but profound. Another view would be that problem and solution fit perfectly. Such a fitting solution has most potential, i.e. it gives headroom for further improvements, which is then an engineering task. We try to examine the different methods from this point of view and want to encourage the reader to do the same.

2. MEASURAND

In order to be able to understand the difficulty of the problem or the elegance of an approach, it is useful to define the measurand, i.e. what we really *want* to measure and what *is* measured in this approach. These questions are not trivial, as we will see; it immediately uncovers the difficulty inherent in indirect methods that compare the principally unknown aspheric surface with a device, whose exact features (including alignments) are only known to a limited accuracy. As a rule of thumb: the more difficult it becomes to follow the chain of arguments, how the aspheric shape is tied to the measurand through the mathematical evaluation of a single or a number of different measurements, the more suspect to all kinds of errors the method might also be in practice. An analogy may be stacks of kinematic mounts or parts that are produced elsewhere individually to specification but are highly suspect in combination.

Despite a family of surfaces, where the asphere is on top of a plane (Schmitt-plate), it usually is on top of a sphere, or in other words, it is a relatively small deviation from a sphere with a certain radius of curvature, see Fig. 1. What should we measure: the shape of the aspheric surface with reference to a plane or the shape of the aspheric surface with reference to the fitting sphere? Let us take an example: if we assume a typical radius of curvature R = 50mm and a diameter D = 65mm, the sag is s = 12mm. Compared to this, the maximal aspheric departure, which might be n_{max} = 0.12mm, is about 100-times smaller. As the absolute uncertainty is the relative uncertainty multiplied with the magnitude of the measurand, we should try to compare against a sphere. The relative uncertainty is more or less a consequence of the specific measurement technique, i.e. it is kind of a feature of this technique and difficult to be improved. So, either you work hard to improve the relative uncertainty, or be clever and reduce the magnitude of the measurand. This is the principle of "measurement by compensation," i.e. like the measurement of a resistance in a Wheatstone-bridge, and it is also the idea behind the null-compensators used in aspheric testing.

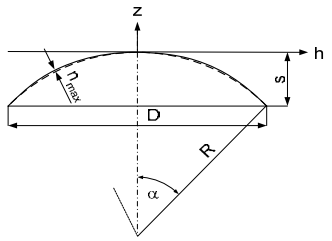

Fig. 1. A spherical surface (dashed) with radius of curvature *R* and diameter $D=2h_{max}$ and a sag s with a rotationally aspheric surface deviation (solid) on top of it together defines the real lens surface; aspheric deviation *n=n(h)*.

As a first guideline towards an elegant solution, we should try to measure in a direction normal to the surface, i.e. in a radial coordinate system rather than in Cartesian *x,y,z* coordinates. A coordinate measuring machine (CMM) approach is already unfavorable from this point of view, if we define as the measurand the aspheric departure from a given sphere and not the radius of curvature *R* as to be our measurand. But if we only measure the aspheric deviation *n=n(h)*, then we have independently to measure *R* in addition, otherwise the measurement would not be complete or even wrong, as the function *n=n(h)* contains *R* implicitly as a parameter. Let us take another view on the problem: assume we compare the aspheric surface with the fitting sphere where the normal deviation *n* is a function of *h*, *n=n(h)*. Then the absolute value of the gradient *dn/dh* is relatively small for all $0< h< h_{max}$, i.e. the error Δn made due to an error Δh in the lateral coordinate *h* is relatively small everywhere:

$$\Delta n(h) = \frac{dn(h)}{dh} \cdot \Delta h \tag{1}$$

We see that *dn/dh* is zero when *n(h)* has an extreme value; i.e. the sensitivity of an error in *n(h)* due to an error in the lateral coordinate *h* is zero there. This is a very favorable condition which we certainly would like to extend over the whole surface, see our method, section 9. It derives from the fact, that the sphere and the asphere have locally mutual normals as both go through the center point of the sphere. The same is true for the apex of the rotationally symmetric asphere; it also has a common normal with the sphere. Assume, our reference sphere would be an optical test glass: then we would get wide fringes in those regions i.e. zero fringe frequency when *dn/dh* = 0.

Now let us go one step back and describe the aspheric surface with cylinder coordinates $z=z(h,\theta)$, with the azimuthal position of a point on the surface being θ. Due to the rotational symmetry of the aspheric surface and the proper choice of the origin of the coordinate system, we see that $\partial z(h,\theta) / \partial\theta = 0$ for each value of h and θ. In other words: the *difficulty* of testing can be reduced dramatically, when clever use is made of the *symmetry intrinsic* to the problem. This symmetry is already used in the mathematical definition of the rotationally symmetric asphere, where the lateral coordinates $x=h\cdot\sin(\theta)$, $y=h\cdot\cos(\theta)$ are substituted by $h=\sqrt{x^2+y^2}$, see for instance Ref. [12] for a superior description or Ref.[14] for the widely used formula for an asphere:

$$z(h) = \frac{c\cdot h^2}{1+\sqrt{1-(1+k)c^2h^2}} + a_4h^4 + \cdots + a_nh^n \tag{2a}$$

defined for $-h_{max} \le h \le h_{max}$

$$c = \frac{1}{R_0} \quad \text{(2b)} \qquad \text{with} \qquad R_0 = \frac{\sqrt{(1+z'(0)^2)^3}}{z''(0)} \qquad \text{Radius of the apex sphere} \tag{2c}$$

$$z'(h) = \frac{c\cdot h}{\sqrt{1-(1+k)c^2h^2}} + 4a_4h^3 + \cdots + n\cdot a_nh^{n-1} \tag{2d}$$

$$z''(h) = \frac{c}{(1-(1+k)c^2h^2)^{(3/2)}} + 3\cdot 4\cdot a_4h^2 + \cdots + (n-1)n\cdot a_nh^{n-2} \tag{2e}$$

Following our discussion of dynamic range, we are now interested in expressing the aspheric departure q with reference to a sphere with a specific radius of curvature $R=R_0+w$; here R_0 is the radius of the apex sphere, see eq. (2c), and w is an additional value, that we might choose. See Fig. 2 for the derivation of the following equations. The value w can be chosen to minimize the maximal absolute value of i or of q, or, as we will see at section 9, $w=w(h)$ can be chosen as a *function* of h such, that i is zero for every h.

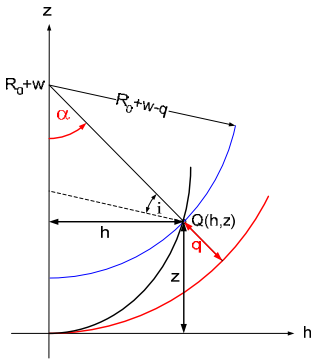

Fig. 2. The center of curvature of a spherical surface (red) is located at a distance $z=R_0+w$ on the symmetry axis of the asphere (black). A point *Q(h,z)* on the aspheric surface has a distance R_0+w-q from this center of curvature. The quantity q is therefore the distance *difference* between the apex and the point *Q* from the center of curvature. Note that q is not normal to the aspheric surface, but it is normal to the spherical surface; the angle between the normals is i. But $i=0$ for that value of w, for which $\frac{\partial q}{\partial h} = 0$, see section 9, our proposed method.

$$q = R_0 + w - \sqrt{(R_0+w-z)^2+h^2} \tag{3a}$$

$$\frac{\partial q}{\partial h} = \frac{(R_0+w-z)\frac{dz}{dh}-h}{\sqrt{(R_0+w-z)^2+h^2}} \tag{3b}$$

$$\frac{\partial q}{\partial w} = 1 - \frac{R_0+w-z}{\sqrt{(R_0+w-z)^2+h^2}} \tag{3c}$$

3. METHODS TO MEASURE ASPHERES

3.1 Basic features of Fizeau Interferometry

Fig. 3 shows a Fizeau Interferometer for testing flat surfaces, windows, convex and concave spherical surfaces and complete lens systems. A key component is the so-called Transmission Sphere (TS), which is a lens system that converts an incoming plane wavefront into a spherical wavefront; the last surface of the last lens element in the TS is made concentric to its focus point. Whereas all surfaces of all individual lens elements are carefully anti-reflection coated for the laser wavelength used for the test, this last surface remains uncoated, therefore reflecting back about 5% of the incoming light, and thus acting as the beam-splitter and the reference surface at the same time. The elegance of this Fizeau principle lies in the fact that no other components than the reference surface and the test surface are involved in establishing the optical path difference. This is called the interferometer cavity (shown red in Fig. 3), and by the laws of interference the optical thickness of the cavity is transformed into an intensity modulation of the interferogram. By methods of Phase-Shifting Interferometry (PSI), this intensity distribution which is gathered with a CCD detector of typically 1k x 1k pixels, can further be transformed in a phase-map, or using the wavelength in air of the laser light source as the scaling factor, rescaled to a height map. As the test surface is imaged to the pixilated detector, each pixel is associated with a ray striking the spherical test surface in an x,y matrix-like raster, and the height map shows the deviations in lengths from a mean value of the rays between the two solid surfaces, the reference surface and the test surface. As the rays all go through the common focal point which is the center of both spheres, they are normal to both surfaces and therefore the lengths of the rays represents the distance properly.

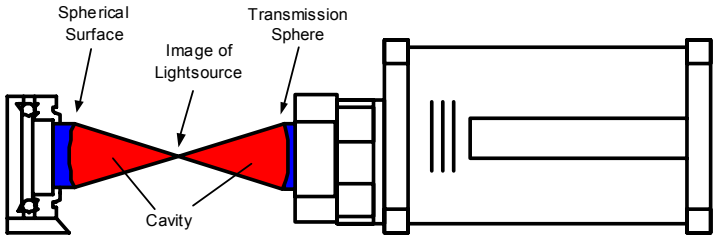

Fig. 3. Fizeau interferometer arrangement containing a mainframe with a HeNe-laser as light source, collimator, beam splitter cube, imaging optics (ocular), and CCD detector. An image of the light source is formed by the TS in its focal plane, acting as a point object for both, the reference surface and the test surface and both surfaces image this object in a stigmatic way into the system aperture located in the common focal plane of collimator and ocular in the mainframe. TS, collimator and ocular form the imaging train that images the test surface with high spatial resolution and only minimal distortion onto the flat detector plane.

This condition is only fulfilled when the alignment of the cavity is perfect, but the real-time nature of the physical interference makes such a near perfect alignment possible. This ability to set-up the test geometry in such a nearly perfect manner is one of the keys to the superior precision of interferometry compared to mechanical methods.

There are other features of the interferometric measurement that contribute to its superior status: these are the *parallelism* of measurement and the *force-free* assessment to the surface. As a consequence of both, there is an absence of any concern about how to close the loop for the measurement force or the like, which is a very important question for a mechanical probe. I want to explain this in a few more sentences: assume that during a series of interferometric measurements the wavelength of the light source would change unnoticed, let us say by 0.1%. This is about 5000-times more, than what could be expected using a HeNe-laser, but we use this excessively large value only to emphasize the argument. Now, as a consequence, the lengths l of *all* rays would *simultaneously* be measured wrong by an amount $\Delta l = 0.001 \cdot l$, which might be as large as 100µm when the radius of curvature of the test surface as well as of the reference surface have been 50mm. But assume, that the height map had shown a deviation of 100nm PV (peak to valley), then the value of the height map would also be changed by 0.1%, i.e. 0.1nm. This small value can easily be tolerated; but what a disaster, if we would have measured the lengths of the rays one by one: now the measurement error would exceed the measurand by a factor of 1000!

Now let us go one step further and assume, the temperature in our measuring room would change by $\Delta\vartheta$=10°C and our interferometer as well as part holder would be set-up on an optical air-supported table made of steel with a coefficient of thermal expansion of α=11.5E-6. The base-distance between supporting points would be 150mm, but if the additional 50mm to the cavity length of 100mm would be made of the same steel as the table, this would be compensated. Then we would experience a length change of the cavity of ΔL = 11.5µm and this would lead to a small misalignment of the set-

up, as now the ray at the center has a different length as the inclined rays at the edge. The mathematical dependency for the extra length Δl in cavity thickness l is easily seen to be:

$$\Delta l(\alpha) = \Delta L \cdot (1 - cos\,\alpha) \tag{4a}$$

and with $\sin\alpha = \frac{h}{R};\ \ \cos\alpha = \sqrt{1 - \frac{h^2}{R^2}}$ we get:

$$\Delta l(h) = \Delta L \cdot \left(1 - \sqrt{1 - \frac{h^2}{R^2}}\right) \tag{4b}$$

where R is the radius of curvature of the test surface and h is the height on the test surface (distance from the center of the surface). This function in eq. (4b) is added to the measured height map due to the axial misalignment of the cavity; as it will show up in the interferogram as a pattern of concentric Haidinger fringes we can easily readjust the cavity prior to another measurement and get the same result for the height map as before the temperature change. But as we could easily calculate this very specific shape, this gives us the possibility for mathematical correction too. As the visual alignment has limited precision to about λ/10 or 60nm, and the phase-measurement of the height-map is at least 100-times more precise, it is in any case necessary to subtract the response functions to misalignments from the final result. This is done by a fit of the shape described by the right hand side bracket in (4b) to the measured height map, using ΔL as a free parameter which is determined by the fit. Again, the inherent parallelism has made us insensitive to temperature changes. But this Gedanken experiment has taught us two additional very important and general valid facts:

1. We lose the ability to measure a surface parameter (here the radius of curvature) when we use this parameter to reduce the dynamic range of the problem.
2. We are blind to all such shapes (modes) of the surface that are response functions of degrees of freedom in alignment.

This second statement might be formulated too general, i.e. is much too pessimistic in cases where we test the whole surface (as one solid body) in one stroke. Then, in cases where the test wavefront is matched to the shape of the test surface, for instance in cases of null compensation, after proper mathematical removal of the misalignment by fitting the response functions to the measured result, finding the amount of misalignment to minimize the residuals and subtracting the misalignment effect, it can be deduced that all *parallel* surfaces to our surface under test would give the *same* measurement result. So we arrange that the solid body is mathematically moved in space until the measured deviation from design shape is minimized. In our case of measuring a sphere in a spherical test set-up, we have initially 3 such degrees of freedom, shifts in *x,y,z*, but then can reduce them to zero, when subtracting the response functions for *x,y,z*-misalignments, however a parallel surface (sphere with a different radius) would give the same measurement result. But this luxury being allowed to remove response functions is no longer given when the final result is composed of measurements of sub-results that are gained with different orientations of the test set-up (stitching). Now the final result needs their proper arrangement in space, i.e. needs a world coordinate system in addition to the coordinate system of the measurement instrument and the intrinsic coordinate system of the test part. If we measure a rotationally symmetric asphere at a subaperture that is not positioned symmetric to the symmetry axis of the surface, we have 6 such degrees of freedom for alignment at every subaperture. As a solid body movement of the subaperture of the part cannot be performed independent from all the other subapertures, a reduction of degrees of freedom is not possible. When 100 such subaperture measurements are needed to cover the surface, we have in total 600 degrees of freedom that will influence the final result.

Using a computer generated hologram for complete or partial compensation of aspheric departure in the wavefront, we have 5 degrees of freedom from the asphere, and additional 5 or 6 degrees from the hologram; some of them might have very similar response functions, so that they may be counted only once, but that makes the alignment task even more difficult. In Refs.[3,44] seven (essential) degrees of freedom have been found for alignment of asphere and hologram. Every degree of freedom produces a characteristic response function that is added to the measurement result, and it is not obvious how to differentiate between some contribution to the surface shape that can be represented by this response function and the identical consequence for misalignment. The fitting of a given function r(x,y) to another function z(x,y) is not a commonly used procedure, and therefore might look unfamiliar at a first glance; a good part of the real surface shape could be reported wrongly when the number of response functions grow. Only degrees of freedom resulting from solid body movements of the *test surface* can be removed without harm (but a parallel surface might then be measured),

but the metrological "stiffness" of a result can be greatly reduced if too many degrees of freedom for misalignment are allowed in total by the concept. It is especially complicated when multiple elements have to work together, like a multi-element null lens, null lens and hologram or partial compensation with measurement of the residual. Most problematic is subaperture measurement with stitching, partial compensation by extra element and measurement of the residual. [27,3,44]

The price that must be paid for the extremely high accuracy of a null measurement in a Fizeau is that we have to measure this radius of curvature in addition, and this is done with a radius bench as shown in Fig. 4. The distance measuring interferometers (DMI) are arranged symmetrical to the optical axis and parallel to the shift direction so that there is no metal in the loop and therefore thermal effects are minimized.

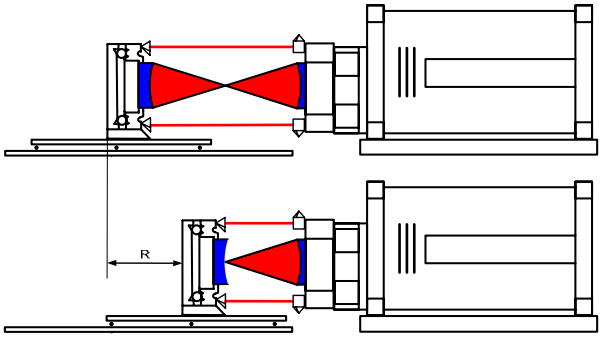

Fig. 4. For measurement of the radius of curvature R of the test surface, two measurements are needed that give an auto-collimation condition i.e. the image of the light source in the focus point of the TS is imaged by the test surface from its center of curvature in the upper drawing and from its vertex in the lower drawing (cat's eye arrangement). The distance that the test surface has to be shifted is the radius R and it is measured with two distance measuring interferometers; the mean value of their readings shows the correct result even when the test surface was not shifted parallel.

4. HIGH DYNAMIC RANGE FIZEAU INTERFEROMETRY (HDRFI)

From the previous discussions it is clear, that by adapting the probing wavefront to the radius of curvature of the aspheric wavefront, we can reduce the measurand to be the aspheric deviation n in normal direction. Only this strong reduction makes it possible, to start thinking to use an interferometer to measure the surface. We will show which difficulties have to be managed in this attempt of high dynamic range interferometric measurements; see also Refs.[27,47,58,59].

Due to the fact, that the rays that all come from the image of the light source (see Fig. 3) do not strike the aspheric surface in normal direction, they are not reflected back into themselves, creating retrace errors. In other words, the local normal of the aspheric surface and the incidence direction of the rays include the angle i, so the angle between incident and reflected ray is $2i$ and the rays cross the optical axis along a line called Caustic; this is the longitudinal aberration of the reflected wavefront, now being aspheric. The best image point of the light source is now found at a position of the circle of least confusion, which defines the minimal lateral ray aberration of the reflected wavefront; its image has to pass the system aperture in the mainframe, otherwise some zones on the test part are not visible on the detector. The interferogram is shown right in Fig. 5. We see circular fringes with different densities. There is one zone, where the radial fringe frequency becomes a minimum; at the very center of the broad ring, it is even zero; the radius h_{zone} of this zone depends on the z-adjustment of the aspheric surface. We find zero fringe frequency again in the center of the part.

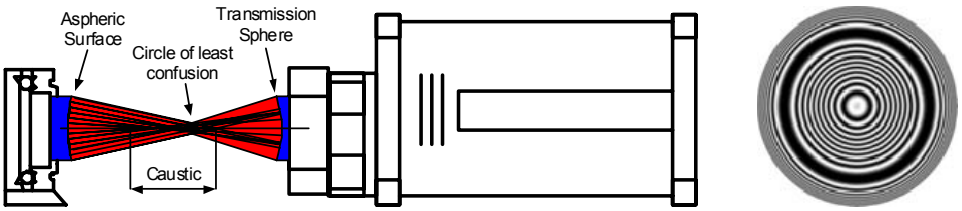

Fig. 5. A mild aspheric surface probed with a spherical wavefront generates an aberrated, aspheric wavefront that leads to high radial fringe frequencies in the interferogram. Optimal adjustment is achieved, when the maximal fringe frequency is minimized; this is the case when the positive and negative gradients have equal magnitude. Shifting the aspheric surface in z-direction changes the radius of the reference sphere for the aspheric departure.

The direct measurement is applicable to mild aspheric surfaces, and we will now first discuss the limits for the aspheric departure and then the main error influences. To simplify our lives and be more specific, we start with an assumption: we assume that the aspheric departure is from a sphere and can be sufficiently described by a term a_4h^4. This is the lowest order asphere and therefore the easiest to be tested. If we would add higher order terms, a_6h^6 or higher, nothing would change in principle, but the max. aspheric departure, which can be tested, would be lower than calculated here. Now we assume, that we use the quadratic term a_2h^2, which can be changed by the z-adjustment of the test surface, i.e. by the thickness of the cavity, to minimize the slope for a given aspheric departure z_{max}, see Fig. 6.

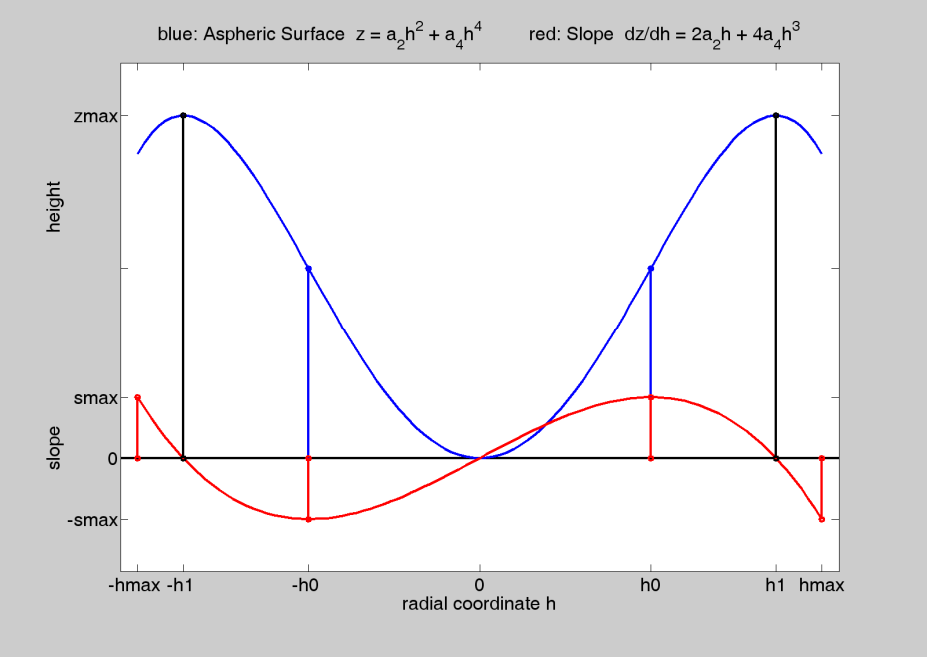

Fig. 6. Blue: the aspheric departure with the optimal balance of a_2 and a_4, see text. Red: for this optimal aspheric shape the slopes at h_{max} and $h_{max}/2$ are equal in magnitude but have opposite signs. For details see text.

The calculation gives:

$$z = a_2h^2 + a_4h^4; \qquad s = \frac{dz}{dh} = 2a_2h + 4a_4h^3; \qquad \frac{d_2z}{dh^2} = 2a_2 + 12a_4h^2 \tag{5}$$

and with the conditions $2a_2h_{max} + 4a_4{h_{max}}^3 = -s_{max}$; $2a_2h_0 + 4a_4{h_0}^3 = s_{max}$; $2a_2 + 12a_4{h_0}^2$=0; $2a_2h_1 + 4a_4{h_1}^3 = 0$; ${a_2h_1}^2 + a_4{h_1}^4 = z_{max}$; we can calculate h_0 and h_1 as well as the values for the coefficients a_2 and a_4 as a function of h_{max} and z_{max}.

We get:

$$h_0 = \frac{1}{2}h_{max} \ ; \qquad h_1 = \frac{\sqrt{3}}{2}h_{max} \tag{6a}$$

$$a_2 = \frac{8z_{max}}{3{h_{max}}^2} \ ; \qquad a_4 = -\frac{16z_{max}}{9{h_{max}}^4} \tag{6b}$$

$$s_{max} = \frac{16z_{max}}{9h_{max}} \tag{7}$$

Taking also into account the detector resolution of the mainframe and the magnification, we simplify our model and only look at the point at the surface with the maximal slope s_{max}. This could be as well investigated when testing an inclined plane surface, which makes the interferometer model somehow simpler. Fig. 7 shows such a strongly simplified model, where the chief ray in point P of the test surface is inclined with respect to the incoming ray by an angle α.

With a number of m pixels across the part diameter of $2h_{max}$ we get an image of the pixel raster on the part surface with a raster constant of $\Delta h = 2h_{max}/m$. The increase in surface height at the most critical part of the surface, where the slope is

highest, is then $\Delta z = \Delta h \cdot s_{max} = \frac{2h_{max} \cdot 16 z_{max}}{m \cdot 9 h_{max}} = \frac{32}{9}\frac{z_{max}}{m}$. The wavefront change Δw is twice that value. For reliable unwrapping in phase-interferometry, one has to stay within the Nyquist criterion; this tells us that the maximal wavefront-change Δw between 2 pixels should be smaller than $\lambda/2$, to be able to decide on the sign of the change. As on a pixilated detector conditions of relative position of fringes to pixels could be unfavorable, and measurement noise and roughness of the surface has to be taken into account in addition, this more theoretical limit is replaced in practice by the condition $\Delta w \leq \lambda/4$. With this condition, that gives us headroom for the roughness and waviness of the part we now can calculate the largest aspheric deviation that can be measured with an interferometer using m pixels:

$$\Delta w = \frac{64}{9}\frac{z_{max}}{m} \leq \frac{\lambda}{4}; \qquad \rightarrow \qquad z_{max} = \frac{9}{256} \cdot m \cdot \lambda \tag{8}$$

Assume m=1000, λ=0.633µm, we get z_{max}=22.5µm; this is a mild (i.e. week) aspheric surface, as stated before. At the interferogram we can count $2\frac{9000}{256} = 70.3125$ fringes between the center and the zone. If you see interferograms measured with less number of fringes, you know, the aspheric surface was even milder. It is interesting to calculate the value for the aspheric coefficient a_4, this is

$$|a_4| = \frac{16 z_{max}}{9 {h_{max}}^4} = \frac{0.04 mm}{{h_{max}}^4}. \tag{9}$$

This value can be used as a guideline for a measurable asphere using the dynamic range of a Fizeau interferometer with 1k x 1k detector.

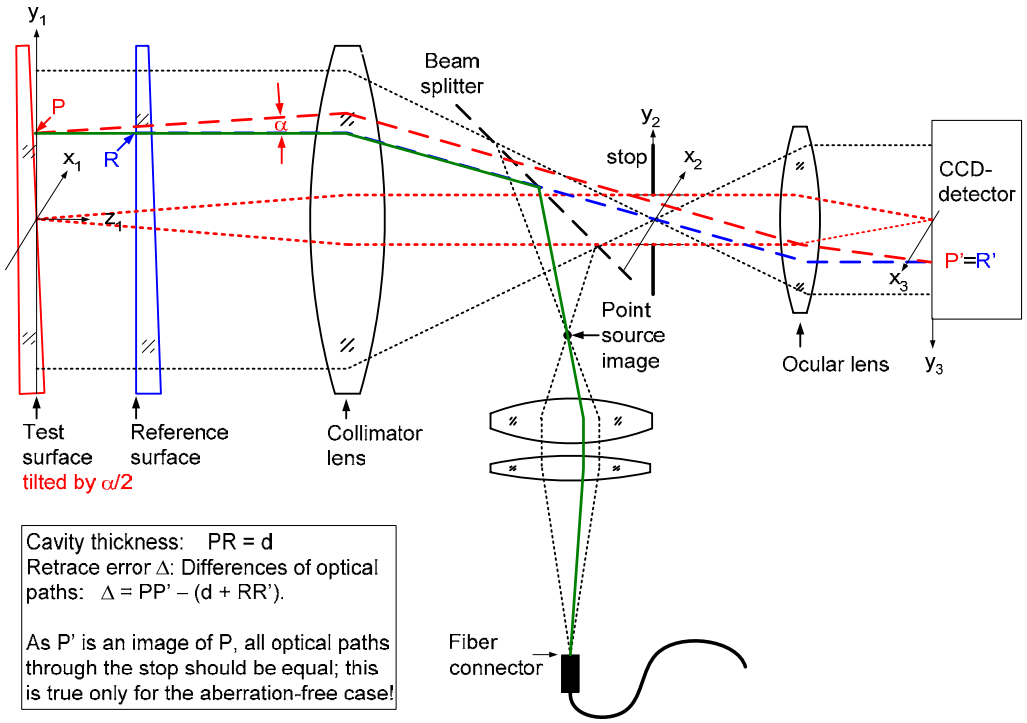

Fig. 7. Simplified interferometer model; the imaging trains consist of two optical systems: the collimator lens and the ocular lens, building a Keplerian telescope. The detector is positioned such, that the flat test surface is imaged onto the flat CCD detector surface. The chief-ray imaging point P on the test surface (red, dashed) and the chief-ray imaging the associated point R on the reference surface (blue, dashed) include an angle α before the collimator lens and an angle α/β after the ocular; β is the lateral magnification given by the ratio of the image size (detector diameter $Ø_d$) to the object size (part diameter = $2h_{max}$). Note: the chief ray has to pass the system's aperture (stop with coordinate system x_2,y_2).

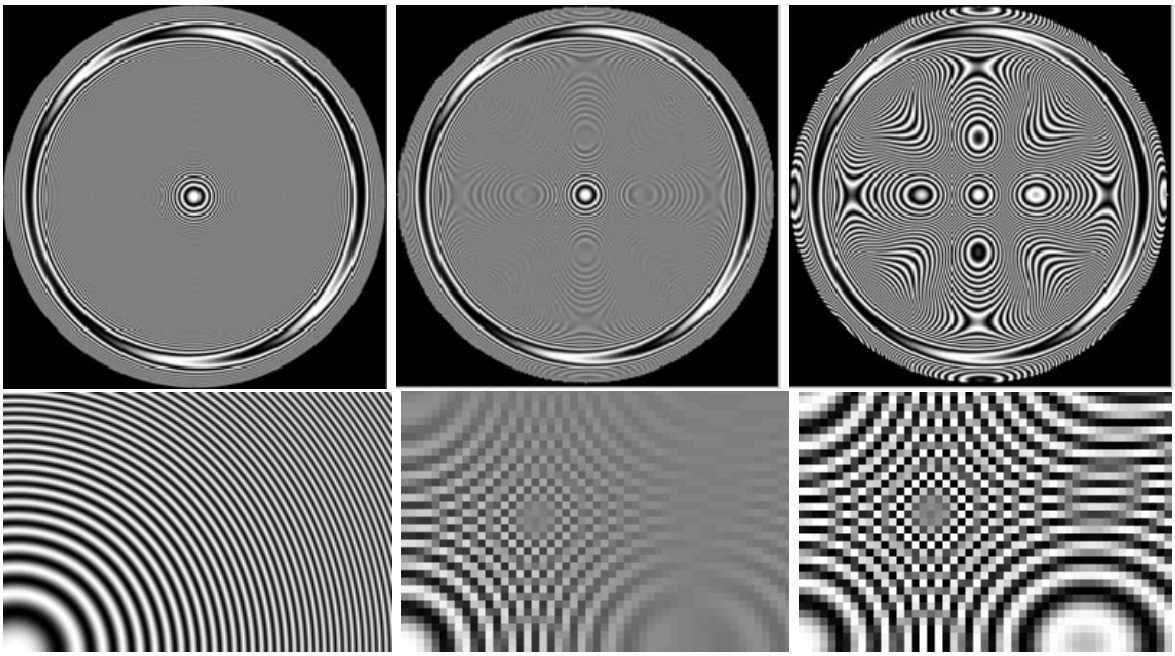

Fig. 8a, 8b, 8c: Interferograms for the example calculated before, i.e. an aspheric departure of z_{max}=22.5µm and 70.3 fringes between center and zone. Fig. 8a: detector with 1k x 1k pixels (0.5-times Nyquist) and a pixel fill-factor of 1 for x- as well as y-direction; fringe modulation is more than sufficient for phase-measurement. Fig. 8b: detector of 250 x 250 pixels (2-times Nyquist), fill-factor of 1; modulation goes through zero, phase reversal. Fig. 8c: detector of 250 x 250 pixel (2-times Nyquist), fill-factor of 0.1 Sensitivity of detector decreased by a factor of 100, roughness of the surface could alias to shape errors.

We have calculated the maximal aspheric departure for an example of a 1k x 1k detector, using 4 pixels per fringe period, i.e. 0.5 Nyquist limit. If a detector with a pixel fill-factor of 1 is used, this leads to a reduction of fringe-modulation by a factor of 0.9, which is acceptable. When instead a detector with only 250 x 250 pixels is used for the same interferogram, two things change: having pixels which are 4-times larger relative to the fringes, the fringe modulation goes to zero, see Fig. 8b. At the same time, the high frequency components in this signal are low-pass filtered by the large pixels, so aliasing caused by the larger spacing is reduced. To avoid the loss of the signal in the high frequency band, the pixels are made smaller, for example a fill-factor of 1/4 is used, bringing them back to the same size as before, so also the same modulation of the signal is retained as before, see Fig. 8c. But now we have sparse sampling of a signal that contains 2-times higher frequency components as can be captured due to the sample theorem, i.e. these higher frequency components are aliased down into the frequency band of the signal that can be represented by this sampling. If we take a simple geometrical model how the interference fringes are built, they can be thought of interference between smooth, inclined surfaces. In the so-called sub-Nyquist interferometry,[32,46] the a-priori assumption is made, that the optical surface as well as its first derivative are continuous; then phase-unwrapping can be performed using extrapolation. But signal theory tells, that every spatial frequency component that is in the frequency band between 0.5 Nyquist and 2 Nyquist will now creep in the result as an error component. Thinking in terms of the images of the pixels on the part surface, these are spatial wavelengths Λ that are larger than 2-times the lateral pixel size and smaller than 2-times the pixels spacing. Especially aspheric surfaces tend to have a ripple structure as a typical error; this combined with a higher roughness than in spherical surfaces is a result of the different conditions of mutual contact (size and pressure in the contact area) between part and tool during polishing. Nowadays detectors up to 4k x 4k are readily available, and detectors with an extra small fill factor are custom made devices, so to me the use of sub-Nyquist techniques seems no longer a preferable alternative to manage high fringe densities. I see the limits set by error sources discussed in the next chapters much more critical than detector resolution. To sum up: a detector with 500 x 500 pixels and 4-times sub-Nyquist with a (linear) pixel fill-factor of 1/8 is equivalent to a detector of 4k x 4k in the conservative case of 0.5 Nyquist. Following our example calculation, they both could measure surfaces with an aspheric departure of 89.6µm from the best fitting sphere. All error sources, that are calculated as examples in the following chapters must be multiplied with a factor of 4 if this would be the goal, in the case of errors by defocus which scale quadratic with slope, even by a factor of 16.

4.1 Setting the cavity thickness correctly

There are not many cases so far, that an aspheric surface is directly measured against a spherical surface, as this alone is a complete solution only for small aspheric departures. [36] When used together with sub-Nyquist techniques, [43] the range of aspheric departure could possibly be increased but at the expense of potentially higher errors, since they scale at least linearly with the dynamic range inherent in the measurement. But also subaperture stitching measures the subapertures against a spherical reference, so this as well falls in this category. In addition, in all cases where the aspheric departure is only compensated partially, the uncompensated remainder is such an aspheric term in the wavefront to be measured, as we will discuss here. In the latter case, it is typically of much higher order [27] and much more challenging than our example calculation for an aspheric departure with a_4h^4.

Most essential for such measurements is, to precisely know the radius of curvature of the (virtual) reference sphere, against which the asphere is measured. This becomes obvious when looking at Fig. 2 and eq. (3a). For a point *Q(x,y)* on the aspheric surface, the measured height map is given by eq. (3a), where zero height is assigned to the apex of the phase-map. This equation is dependent on *w*, which is a quantity used for optimizing the fringe density, i.e. the wavefront slope *i*. If *w* contains an error *Δw*, one get a characteristic error in the measured height map according to (3c):

$$\Delta q(h) = \frac{\partial q(h)}{\partial w} \cdot \Delta w = \left(1 - \frac{R_0+w-z(h)}{\sqrt{(R_0+w-z(h))^2+h^2}}\right) \cdot \Delta w \tag{10a}$$

Inserting (2a) into (10a) and performing a series expansion in h^2 up to h^6 gives the following polynomial:

$$\Delta q(h) = \left[\frac{1}{2(R_0+w)^2}h^2 + \frac{R_0+4w}{8R_0(R_0+w)^4}h^4 + \left(\frac{{R_0}^3+6w{R_0}^2+12w^2R_0+2w^3}{16{R_0}^3(R_0+w)^6} + \frac{k}{8(R_0+w)^3{R_0}^3} + \frac{a_4}{(R_0+w)^3}\right)h^6 + \cdots\right] \cdot \Delta w \tag{10b}$$

This error function is dependent on *w* as a parameter, and scales with *Δw*. There is no way, to mathematically judge, whether this characteristic function stems from an error in the manufactured surface or from an axial misalignment of the set-up by *Δw*. In Ref. [36] the optimal alignment is found by minimizing the residual between design and measurement, i.e. the method is intentionally blind to the type of response-function as given in (10). In Ref.[43] no comment is made about the correct set-up and the consequences for the measured aspheric shape if *w* is taken wrong, which, as can be seen from (10b), does not only contain a "power" term with h^2.

The problem could be solved by measuring the apex distance of the aspheric test surface from the center of curvature of the reference surface. This could be done with the cat's eye measurement shown in Fig. 4 in the lower figure; then the test surface is shifted in the radius bench by R_0+w which is calculated beforehand as the optimal position for minimizing the maximal wavefront slope. A calculation according to eq. (10b) is done during the establishment of the error budget to calculate the specific contribution of an error *Δw* to the uncertainty.

4.2 Magnification and distortion in the imaging leg

We always have to solve the task, to associate the coordinate system of the measurement device with that of the design surface: this is a problem of matching two surfaces together, the *design* surface $z_d(x_d,y_d)$ and the *measured* surface $z_m(x_m,y_m)$. Rigid body movements (alignment) have been discussed; now we look at already centered coordinate systems. Looking at Fig. 8 and the associated Fig. 6, we see that the highest fringe density occurs at the max radius h_{max} and at half the maximal radius, at $h_{max}/2$. When the imaging train, consisting of the TS lens, the collimator lens and the ocular lens produces radial distortion of the image, then the fringes are dislocated and therefore the wavefront has a different height value at this point. Notice: when a nulled interferogram is measured, the wavefront slope is approximately zero everywhere and magnification as well as distortion can do no harm.

From eq. (7), $s_{max} = \frac{16z_{max}}{9h_{max}}$, we calculate for the error Δz in the measured height due to an error Δh in the location where we measure:

$$\Delta z_{max} = s_{max} \cdot \Delta h = \frac{16z_{max}}{9h_{max}} \cdot \Delta h \tag{11}$$

Let us assume 1% distortion, i.e. $\frac{\Delta h}{h_{max}} = 0.01$ (this can be a small number, taking into account the complicated design of a TS with high NA), then we get:

$$\frac{\Delta z_{max}}{1\%distortion} = \frac{16}{900} Z_{max} \tag{12}$$

This is about 1.78% of the maximal PV departure of the surface, which is by no means negligible. For our example of Fig. 8 with z_{max} = 22.5µm, we would get a measured height error of 400nm. As the distortion can easily be >1.5%, this measured surface height error could be larger than 1λ.

I have not discussed here, how such a distortion function can mathematically be described by a certain polynomial enabling the calculation of error propagation when an aspheric departure from the basic sphere is measured; the reader might do this exercise. But it is obvious, that the *first* requirement for evaluating the measured wavefront and associating this with the part under test is the precise knowledge of the imaging *magnification M*, which we define by:

$$M(h_{pix}) = \frac{h_{pix}}{\sin\alpha} = A_0 + A_2 \cdot {h_{pix}}^2 + A_4 \cdot {h_{pix}}^4 \tag{13a}$$

$$M(\sin\alpha) = \frac{h_{pix}}{\sin\alpha} = B_0 + B_2 \cdot (\sin\alpha)^2 + B_4 \cdot (\sin\alpha)^4 \tag{13b}$$

In these definitions of magnification M the distortion is included and we use one of the two forms, either if the aperture angle sinα in object space is given and we want to calculate the associated height of the image in units of fractions of pixels (i.e. h_{pix}), or when the image height is given and we look for the associated numerical aperture. Note that

$$h = (R_0 + w)\sin\alpha \tag{14}$$

I think that the reader can see that precise knowledge of magnification and distortion are important and must be carefully taken care of, when this technique of direct measurement of an aspheric surface is envisioned. The only way to do this reliably is to measure the magnification and distortion [57], which is another topic and shall not be discussed here. Using design values to calculate distortion does not take into account tolerances in the as-built system and actual set-up. It should be noted, that in the general (as-built) case, magnification and distortion is no longer a one-dimensional function of h_{pix} or $\sin\alpha$ only, but depends in addition on the azimuth θ, or should be expressed in x_{pix} and y_{pix} and associated dimensionless coordinates in object space.

4.3 Retrace errors

Retrace errors are another error source in Fizeau interferometry, when it is applied to a high dynamic measurement. Retrace error compensation has been published in Ref. [45] using Zernike functions for the description and compensation of the errors. Practically, they cannot be easily differentiated from distortion errors, which further complicate things. We come back to Fig. 7 to explain their origins using ray-optics. As we can see, point P' on the detector is an image of point P on the test surface. In an ideal optical system, all rays from object point to image point have equal optical path lengths; the deviation from this condition in real optical systems is called the wavefront aberration. For a given field coordinate of point $P(x_1,y_1)$, it can be characterized by the aperture coordinates (x_2,y_2) that the chief ray emerging from $P(x_1,y_1)$ has. These aperture coordinates are proportional with the local surface slope $\frac{\partial z(x_1,y_1)}{\partial x}$ and $\frac{\partial z(x_1,y_1)}{\partial y}$ of the surface point, and when x_1,y_1 change, the slope changes and the aberrations change as a consequence. Therefore retrace errors can be defined as an extra OPD that is not caused by the surface height $z(x,y)$ but by the surface gradient $\nabla z(x,y)$. This part of retrace errors could be found by ray-tracing, if the geometry would be known precisely. There is another part of the problem, which stems from the imperfect alignment of the components and from all individual lens surfaces and inhomogeneity of material used to manufacture the interferometer. As long as reference ray and object ray are strictly superimposed, there is no chance for an optical path difference to be introduced between them, even when the parts would be of very low optical quality; but the larger the shear between the rays, the larger the introduced OPD. This second function is of mid- to high-spatial frequency in nature, i.e. it cannot be described by aberration polynomials. It acts essentially as a coherent noise floor that is added to the measurement in regions of high wavefront slope. The effect is mitigated by the ring-source in Zygo's interferometers [41,54], but not completely eliminated.

It is important to notice, that the retrace errors are a function that depends on 4 variables, x_1,y_1,x_2,y_2, see Fig. 7. The largest part of the retrace error stems from the TS lens, as these lenses are high NA and therefore cannot be corrected for object field perfectly at the same time. But unfortunately, the amount of aberration is also strongly dependent on the radius of curvature of the test surface, as this influences the actual bundle diameters in the TS at every surface. Taking the ratio $\rho = \frac{R_R}{R_T}$ of the radii of curvature of the reference surface to the test surface as another parameter, we have a function of 5 independent variables:

$$\Delta = \Delta(x_1, y_1, x_2, y_2, \rho) \tag{15a}$$

$$\Delta = \Delta(x_3, y_3, x_2, y_2, \rho) \tag{15b}$$

To measure this function, we have only access to the image, which has the coordinates x_3,y_3; therefore, we replace (15a) by (15b). Practically, different lateral shifts of different spherical test surfaces have to be combined for the evaluation of this function. It is in particular *not sufficient* to use a spherical surface and shift this along the optical axis and measure the effect of the increasingly introduced spherical aberration. In this case, the fringe density is increased in a very specific fashion characterized by the Fresnel law, i.e. the coordinates are not varied independently. If this simplified technique is used to generate a correction function for an aspheric test as described in [43], the result is flawed.

Measurements have shown that the retrace errors, if remain uncorrected, easily can reach 0.5µm surface error, when a TS with F/ 0.75 or higher NA is used, even when the tilt is restricted to 0.5 Nyquist and $\rho<2$. They scale very much with ρ; the general advice is, to adapt the radius of the TS to that of the test part as close as possible; reasonable results are still obtained for $1 \leq \rho \leq 5$, for $\rho > 10$ the errors become excessive.

In order not to extend the length of the manuscript too much, we want to restrict our considerations of retrace errors here to what was said, but we want to emphasize, that this is an important source of errors and one of the many restrictions for the use of Fizeau interferometry in all cases, where high fringe density is involved. This is not only true in the application discussed here, but especially when stitching subapertures of aspheric surfaces in a general manner. Here the problem is especially difficult, since every interferogram shows a fringe pattern with different orientation and fringe density in different areas and rotational symmetry no longer exists. If not carefully corrected, the result in every subaperture is altered differently by retrace errors and these many errors are not only linearly propagated, but due to the principle of stitching with the help of overlapping areas, are amplified.

4.4 Residual focus error when imaging the test surface onto the detector

A non-perfect imaging of the curved test surface onto the flat detector surface is the most troublesome error source in high-dynamic range interferometry. Defocus is another aberration of the imaging leg like the others, but it is dominant and it cannot be made zero. The reason is that when the flat detector (image plane) is imaged back into the object space, where the test surface is located, in the best case it will match partially with the shape of the test surface. Ignoring the aspheric deviation (which is small compared to the spherical shape of the test part, see Fig. 1), the ideal case would be, that the detector image in object space would be curved just the same way, as the object surface is curved; then no defocus would occur. This should be true for all different test radii, and also for concave as well as convex surfaces, that all can be tested using the same TS. Unfortunately by first principles such a design of a mainframe and TS is not possible. The best what can be done is to design the imaging train such, that the flat detector surface is imaged into a flat image; generally, this ideal condition will not be reached. Now this flat image can be shifted (by shifting the detector) to intersect with the surface to be tested. The best focus setting is achieved when the intersection is halfway between the regions with highest slope, and this is at $0.75h_{max}$, see Fig. 6. In practice, there are no means to set the focus precisely to that space. Now let us discuss what the quantitative consequence of an error in the focus setting is. We will see that this error scales linearly with the amount of defocus, but quadratically with the surface slope.

Fig. 9 shows the situation on two different parts of the same detector. At the left hand side we see an enlarged portion of the detector, where the rays from the reference surface (black) and the rays from the test surface (red) are parallel, i.e. the surfaces have been parallel too, and when the rays interfere, there will be a region of wide interference fringes. The measured phase-difference does not change in this region from one pixel to the next. It might be the region at $h=0$ or at $h=h_1$ in Fig. 6 and Fig. 8. If we slowly shift the detector by an amount $\Delta z'$, i.e. change the focus setting, the measured phase-difference will not change at these regions and no fringes are there to move right or left; this is characteristic for a nulled interferogram, that the phase-result is insensitive to defocus. Now we compare the situation at the right hand side: here we have the image of a part of the test surface, which shows a high slope with respect to the reference surface, for instance the portion of the wavefront with $h=h_0$ or $h=h_{max}$, shown in Fig. 6 or Fig. 8. Notice, that the slope in h_0 is positive but the slope in h_{max} is negative, so the angle that the red arrows built with respect to the black arrows will have different signs too. Assume that the slope is such, that the OPD between neighboring pixels is Δw. Now see again, what happens, when the detector is slowly shifted by the amount $\Delta z'$ shown in the figure to the position of the dashed line: we also would change the interference OPD by Δw, but only in the regions of high slope, i.e. the fringes would move here. In regions of zero slope no fringe movement, i.e. the original path-difference (i.e. interference phase) would be still there.

As a consequence, phase-values are altered with a speed proportional to the slope including the sign, and the measured surface *shape* changes dramatically, but the measured PV value is kept fixed.

I have made this experiment to measure a mild aspheric part twice and changed the focus of the mainframe in between by a non-controlled, but considerable amount. The difference in the measured OPD showed a PV value of 14µm! This occurred at the parts of the surface with highest slopes.

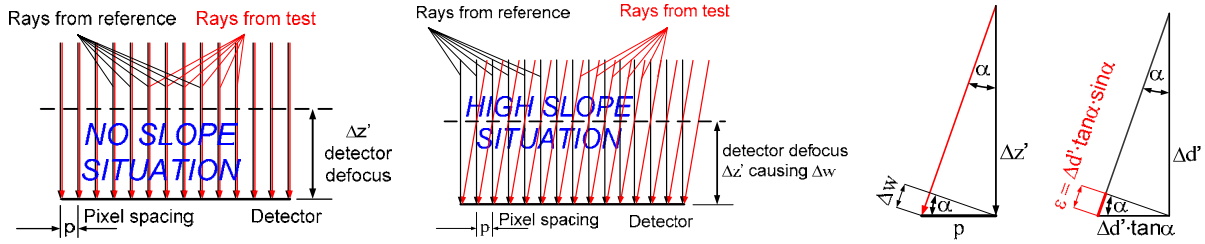

Fig. 9a, 9b, 9c, 9d: Schematic sketch to explain OPD errors introduced by defocus in regions with no slope (9a) and high slope (9b) between test surface and reference surface. The pixel spacing is p and the OPD-change between neighboring pixels is Δw in the regions of high slope. A shift of Δz' of the detector changes the OPD by Δw in regions of high slope but at regions of no slope, the OPD keeps unchanged. Fig: 9d: from similar triangles, we see that a defocus Δd' in the image causes a wavefront error ε.

In interferometry, the depth information in the wavefront, for instance z_{max}, is preserved from object to image, the lateral dimensions of the test surface are scaled with the magnification β, axial dimensions of the test surface with the square of the magnification, β^2. When the wavefront slope is defined as wavefront-increase per pixels, we calculate:

$$\sin\alpha = \frac{\Delta w}{p} \tag{16a}$$

From Fig. 9d we see that a defocus $\Delta d'$ at the detector causes a wavefront error ε that is calculated as:

$$\varepsilon = \Delta d' \cdot \sin\alpha \cdot \tan\alpha = \Delta d' \cdot \frac{\sin^2\alpha}{\sqrt{1-\sin^2\alpha}} \tag{16b}$$

For small values of sinα this is:

$$\varepsilon \approx \Delta d' \cdot \sin^2\alpha = \Delta d' \cdot \left(\frac{\Delta w}{p}\right)^2 \tag{16c}$$

Expressed with the equivalent change of the focus position Δd in object space gives:

$$\varepsilon \approx \beta^2 \cdot \Delta d \cdot \left(\frac{\Delta w}{p}\right)^2 \tag{16d}$$

The amount of defocus Δd in object space that keeps the associated measurement error smaller than ε is given by:

$$\Delta d \leq \frac{\varepsilon}{\beta^2} \cdot \frac{1}{\left(\frac{\Delta w}{p}\right)^2} \tag{16e}$$

Let us take an example: for a pixel spacing of p=7.4µm and our maximum allowed wavefront slope of 0.5 Nyquist, $\Delta w = \frac{\lambda}{4} = 0.158\mu m$ as well as a test surface of diameter D=65mm and 1k x 1k detector, we get $\beta = \frac{1000 \cdot p}{65mm} = \frac{7.4}{65}$, and finally:

$$\Delta d \leq 0.169 \cdot 10^6 \cdot \varepsilon \quad \text{(for max. slope defined by 0.5 Nyquist)} \tag{16f}$$

Now let us assume that we are so ambitious to use the same detector with 4-times Nyquist, i.e. $\Delta w = 2\lambda = 1.2656\mu m$. Keeping all other things the same as before, we get:

$$\Delta d \leq 2.638 \cdot 10^3 \cdot \varepsilon \quad \text{(for max. slope defined by 4 Nyquist)} \tag{16g}$$

If we restrict the max. allowed wavefront error by only this influence (there will be more from other error sources) to λ/10 which means λ/20 for the equivalent surface error, we get for the 0.5 Nyquist case $\Delta d \leq 10.683mm$ and for the 4 Nyquist case $\Delta d \leq 0.167mm$. When we look at figure 1, we see that the sag s of the part is 12mm, i.e. with setting the focus at the optimal position, we just could stay within the limit for the 0.5 Nyquist case; for the 4-times Nyquist case,

there is no chance to fulfill the requirement. In other words: the measured shape of the surface will be altered much more than allowed. This is a result of the quadratic dependence of this error from the wavefront slope at the detector.

We will see later, that null-correctors are used to measure aspheric departures as large as 1mm; in this case, the chief rays from test part as well as reference surface falling onto the detector are made parallel, so a shift of the detector influences the blur-spot and also the appearance of mid-and high spatial frequency features, but not the measured shape.

5. ZONAL STITCHING USING THE SYMMETRY

Looking at Fig. 5, we see that the optical path difference in the cavity is changed in a different manner for different zones of the test surface, when the surface is shifted along its symmetry axis; this can also be seen by looking at Fig. 2, as q depends on w. The zone with broad interference fringes will always occur when the rays strike the aspheric surface in normal direction. This is the case, when the center of the spherical reference surface coincides with the point, where the normal of the aspheric surface strikes the symmetry axis, see Fig. 10.

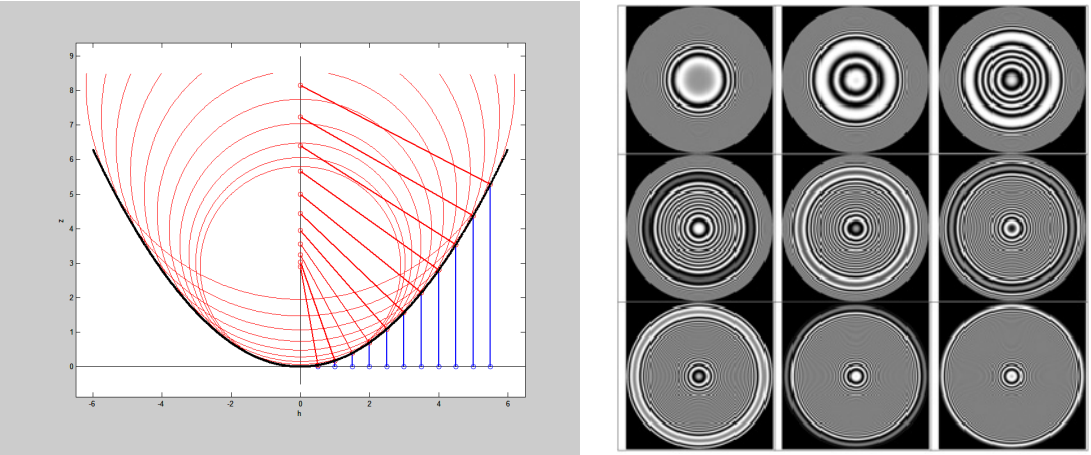

Fig. 10: The normals to an aspheric surface strike the optical axis along a certain line; when the center of the spherical reference surface is placed at a certain point on this symmetry axis, the geometrical distance-change to the asphere as a function of h becomes twofold zero, i.e. a zone with broad interference fringes appears there.

Now, when the w-distance is changed in small steps, an ensemble of zones can be measured, where every zone shows in the ideal, error free case the deviation $q(h)$ of the aspheric surface from a sphere with the radius (R_0+w) as given in (3a). Subtracting the theoretical deviation as given in (3a) would lead to the remainder, which is the deviation of the measured surface from its theoretical value in (almost) normal direction, if only the broad part of the zone is used. But this technique requires that w is measured carefully, otherwise the design value for the measurement is not well defined.

$$q = R_0 + w - \sqrt{(R_0 + w - z)^2 + h^2} \tag{3a}$$

From the right hand side of Fig. 10 one can see that the zones become smaller at the larger diameters. This depends on the special asphere as will be explained later, but is often the case; so the measurements are chosen more densely there.

Now, there have been several attempts to use this nice feature that the measurable part can be shifted over the surface for a metrology on the asphere.[4,6,15,16,17,21] All these techniques use stitching to combine the results of the individual zonal measurements. As the authors do not base the analysis of the residual errors on the measurement of w, but instead use the conditions derived from stitching to determine the first three degrees of freedom of annular zones (piston and 2 tilts) to make the surface continuous, the results must remain defective. In addition, the difficulty in stitching these interferograms together might easily be underestimated: the magnification $M(h_{pix}) = \frac{h_{pix}}{\sin\alpha}$ as defined in eq. (13) is a function of the scan position w in addition, as this changes the aperture angle α to a point, see Fig. 11. Therefore also the lateral coordinate changes from one interferogram to the next, and a simple sewing together the partially overlapping phase-maps must lead to severe errors in the final result, see Fig. 11. In addition, to handle the inherent difficulties, the authors

used a fitting to annular Zernike polynomials as the substitute for their measured phase-maps, so that all higher spatial frequency information that especially is easily attained along each circle in the center of a zone was lost.

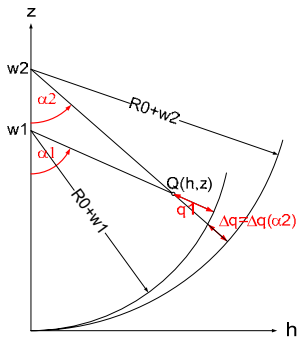

Fig. 11: The same point *Q(h,z)* on an aspheric surface leads to different measured height deviations with respect to the apex, q_1 and q_2, when the scan position was changed from w_1 to w_2. But in addition, the point *Q* appears at different pixel locations, since the line of sight along the ray, has changed its (aperture) angle α with respect to the optical axis too.

If we again count the degrees of freedom that are inherent in this measurement approach, in order to see to what the method is blind, we get three degrees (Δx, Δy, Δz) for every zone; if for example 12 zones are measured, we will count 36 degrees in total. It might be possible to decrease this number for using the stitching to remove the consequences of Δx, Δy, which are different amounts of tilt in every zone. But the real challenge in measuring rotationally symmetric aspheres is to measure their aspheric profile; this target is missed here, since the remaining 12 uncertainties in the z-position allow nearly every shape of a profile to come out. An additional severe drawback of this approach is that the zones must be relatively broad to allow stitching. Therefore in the patent Ref.[21] a special device was installed in the interferometer illuminating beam to adapt the wavefront onto the shape of the annular zone, using as many devices as zones. From our considerations of degrees of freedom it is clear, that this again may have the unintended consequence of increasing the uncertainty of each zone.

6. GENERAL STITCHING WITHOUT UTILIZING THE SYMMETRY

To explain the motivation not to use the inherent symmetry in the problem for the stitching procedure, as it was described briefly in the chapter before, we will introduce the evolute [29] of an aspheric surface with the help of the following Fig. 12.

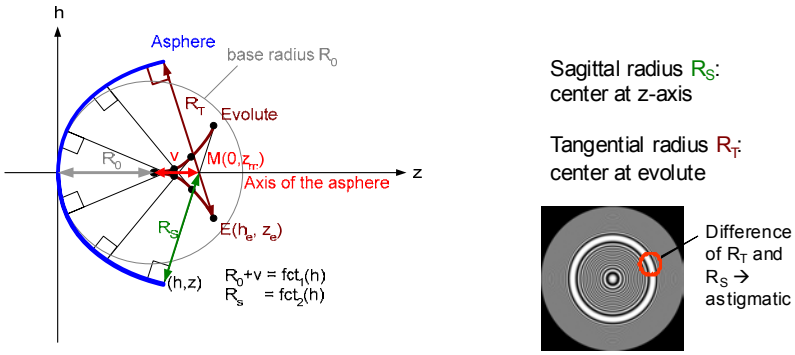

Fig. 12: The aspheric surface (blue) has an evolute (brown). A point $E(h_e,z_e)$ on the evolute is the center point of a sphere, that matches the shape of the asphere in tangential direction, creating a 4-fold matching point; the radius of the matching sphere is the tangential radius R_T. The tangential radius crosses the z-axis (symmetry axis) in a point $z=R_0+v$. This is the center of another sphere that matches the aspheric surface in a parallel of latitude, i.e. in sagittal direction, the radius is R_S. The length-difference $|R_T-R_S|$ of these radii defines the amount of astigmatism, that this point of the aspheric surface has.

Assume, that we position the aspheric surface before our spherical Fizeau such, that the center of the TS coincides with point M in Figure 12; then we see an interferogram as shown on the right hand side. This is the symmetrical case, as we are used to already. With a stronger asphere, the zones become very narrow; zooming in the whole interferogram does not solve the problem, because the zone would appear larger and larger in diameter, and finally disappear. To overcome this problem, one could decide to look at a certain azimuthal region of the zone; this now can be zoomed in to fill the complete detector. Practically, this is achieved by using a TS lens with much lower NA, i.e. longer focal length. The magnification as defined in (13) is now much larger than before. As a consequence, fringes are now resolved that were unresolved before. If now the distance to the surface is changed such, that the center of the reference surface coincides with the point $E(x_e,z_e)$ in Fig. 12, then the appearance of the fringes changes, as now the lateral direction shows nearly no fringe density, in the sagittal direction the measurable field is decreased in return. In an axial position somewhere in between these extremes, the measured height-map looks like a saddle, and the overall fringe density is minimized. This is the condition, which is seen as ideal for stitching.

Fig. 13 shows as an example 4 interferograms that are typical for stitching and are calculated on a relatively mild asphere that easily could be measured with Zygo's VeriFire Asphere machine in the axial symmetrical way. In all 4 interferograms, the position of the center-point of the TS lens relative to the aspheric surface is changed only very slightly, in the scale of Δx=5µm lateral shift between the columns and Δw=50µm axial between the lines in the below 4x4 matrix, the aspheric surface has not changed. As can be seen from the interferograms in the red circles (this is the subsection, which the interferometer will see), the height maps are quite different in the scale of the needed uncertainty of nm. But there is no way to decide from the measurement result, whether the measured height map has this shape due to the relative orientation of the reference surface, or whether the surface itself contains this component. If we have no precise outer world-coordinate-system, we can only try to mitigate this problem, but not solve it profoundly.

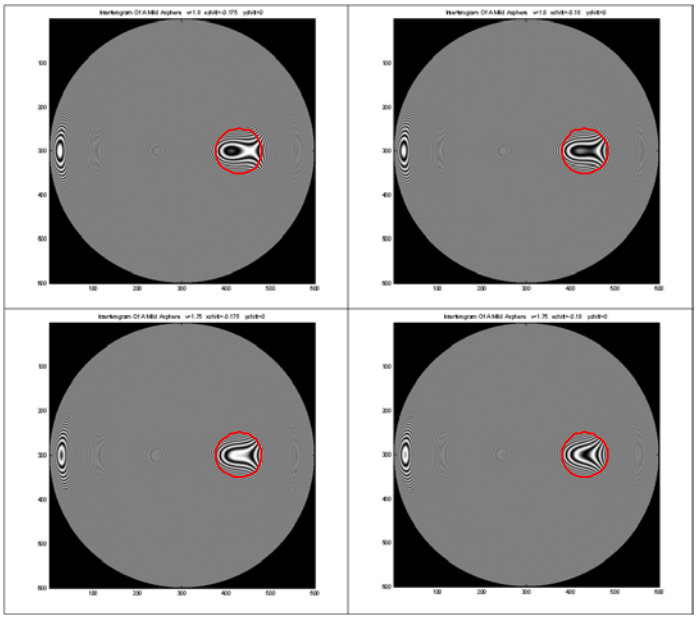

Fig. 13: The same subaperture of a mild asphere is tested with different positions of the center of the spherical reference surface; this center was shifted between the two columns by 5µm in horizontal direction and the radial distance was changed between the upper and lower interferograms by 50 µm.

A known method applied to this problem is stitching of overlapping measurements, which as will be shown here, is reasonable for spheres but is less than ideal for aspheres. The basic idea behind traditional stitching methods is that, because of the high number of measurement points that Fizeau interferometry is able to produce in parallel in a fraction of a second, redundant information is produced. In the overlapping areas it is known that the surface is the same even when the test part has changed its position and therefore homologous surface points are found in different locations on the detector. Let us assume that the knowledge of the world-coordinate system in which the global orientation of the test surface relative to the reference surface is traced would be known precisely enough (let us say to 5µm in the three lateral

degrees of freedom and with matching precision for the 3 angles) to associate homologous surface point-pairs. Then there is still the problem that the test surface and now 2 relative orientations of the reference sphere to the aspheric surface are simultaneously unknown. If we get rid of one set of unknowns by this double measurement, there remains one set of unknowns that cannot be separated. In other words: if we would subtract the two measurements, then the unknown test surface would drop out and from the remaining difference map we could only see the *change* in orientation, but not decide on the *absolute* starting values; these have cancelled by the subtraction. Fig. 14 shows such a situation, where the test part has been shifted relative to the reference surface to show a new field for the measurement. The height map can be measured in the light blue circle in the interferogram left, and in the red circle in the interferogram right. The overlapping region is large in this case (>50%), but it is impossible to get rid of the influence of the degrees of freedom for alignment. In the stitching software, these degrees of freedom are introduced and left as free parameters for a final, global solution of a system with a very large number of equations.

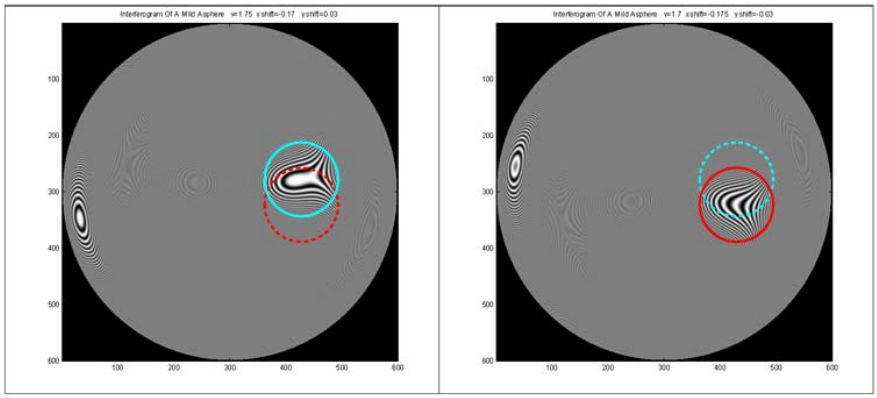

Fig. 14: Stitching two measured height maps together in the overlapping regions; for details see text.

The amount of aspheric departure that can be measured with the stitching approach naturally must find a quite hard limit, as two effects amplify each other to restrict the applicability of this method: when the aspheric surface gets steeper, the diameter of the subapertures must be reduced to get resolvable fringes and at the same time their number has to be increased quadratic to cover the whole surface with the smaller areas. So the number of degrees of freedom is quadratic increased and as a consequence, the error propagation will become more unfavorable. In addition the measurement time is increased, which together with drifts in the mechanical structure increases the measurement uncertainty, especially of the world coordinate system. There are all the error influences discussed with high dynamic Fizeau interferometry in section 4 now in every measurement, like the knowledge of magnification and distortion, retrace errors, and residual focus errors. These errors, as never be removed by calibration measurements to 100%, will print through in every measurement to some extent, and as they depend on the measured height map in addition, it will not be possible to remove them in a global way at the final calculation to best match all measurements in a least square sense. On the contrary, they will be trouble makers till the final result.

Knowing from own experience, how quickly all equations become complicated and confusing in the general, 3-dimensional case including part errors, and even the theoretically given designs cannot always be calculated with sufficient precision [48], I have the highest respect for the scientific and engineering work related to this technique [34,42,47], but I see the basic approach as not well suited to aspheric surfaces. Stitching of spheres and planes [30] is a totally different story: here stitching has great potentials, since the interferometer is always used at its superior conditions so the errors in each measurement are smaller by orders of magnitude. Other work includes stitching of large x-ray synchrotron mirrors [31]; here one dimension is much less aspheric than the other.

An approach to compensating the local aspheric departure would be a variable null compensator placed between the aspheric subaperture and the TS lens, in order to compensate part of the aspheric departure as seen by the interferometer [56]. The dominating aberration in a subaperture is Astigmatism, next comes Coma. When these aberrations are introduced by the compensator with opposite sign, they are cancelled in the measured wavefront and as a consequence, a subaperture with a larger diameter can now be tested, before the fringe density at the subaperture edges becomes too

high. Figs. 15a, b, c, d show a subaperture at h=80mm with a diameter of d=18mm of a steep aspheric surface with a diameter of 175mm and 1.387mm departure from the fitting sphere.

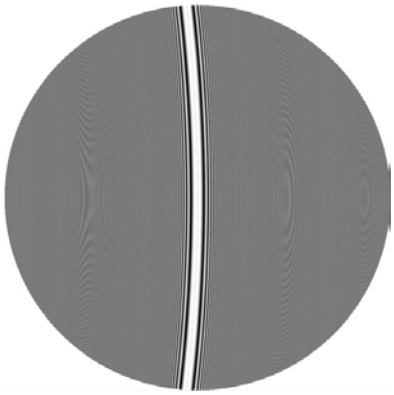

Fig. 15a: Steep aspheric surface tested with the center of the reference surface located on the symmetry axis: zonal test, see Fig. 12. A subaperture with 18mm diameter is shown.

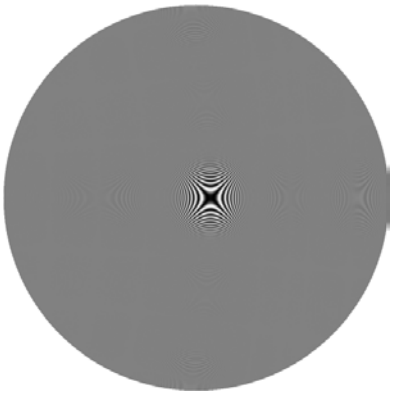

Fig. 15b: Same 18mm subaperture, but now the center of the reference surface is shifted along the normal away from the symmetry axis and has a radius of 0.5(RS+RT). PV = 332µm

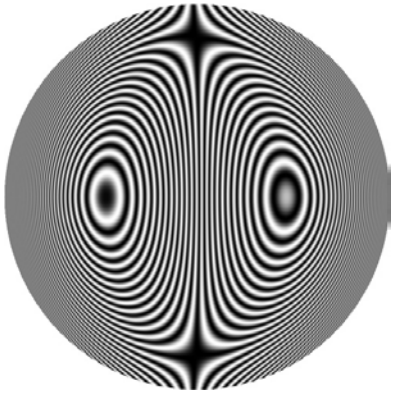

Fig. 15c: When astigmatism contained in 15b is compensated, a much lower fringe density results, but still fringe density on the edges is very high. PV = 24.5µm.

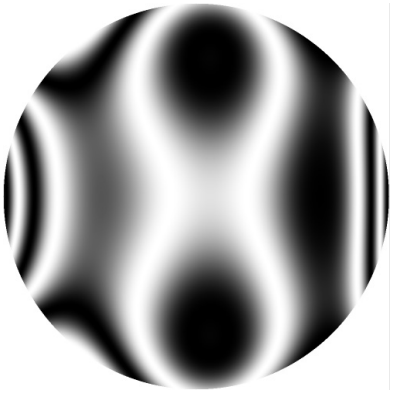

Fig. 15d: When Coma is compensated in addition, a low fringe density results. Now a test could be performed with relatively low interferometer induced errors. PV = 1.694 µm.

There are very many possibilities for a subaperture Astigmatism compensator, for instance a bending mirror [56] or a pair of cylinders that can be rotated against each other. But as can be seen from the examples, it is required that Astigmatism as well as Coma can be compensated independently, but at the same time. This is more challenging, but also several solutions can be thought of, for instance a symmetrical optical 1:1 relay system of 6 elements as shown in Fig. 16a. This system produces very strong field dependent astigmatism, i.e. continuously growing amount of Astigmatism can be introduced by tilting the system, see Fig. 16b; Coma is introduced in addition by decentering (lateral shift) the two symmetrical half-systems with respect to each other.

Even simpler solutions are shown in Figs. 17a and b as well as Fig. 18a and b. Here two respective three spherical mirrors are used under oblique incidence to simultaneously produce Astigmatism and Coma. Parameters for the design of these systems are the radii of curvature of the mirrors as well as the incidence angles; a plane wave enters the system. The simplicity of this design allows superb calibration of component errors. In Fig. 17b and 18b the remaining errors for a 20mm diameter subaperture are given for the same example as shown in Fig. 15 for an 18mm diameter subaperture.

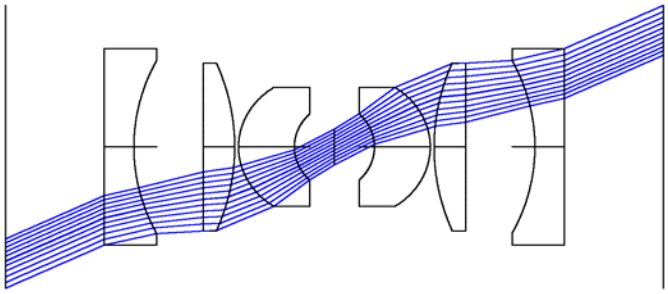

Fig. 16a: A proposed continuous compensator for Astigmatism and Coma; tilting about the symmetry center increases astigmatism; lateral shifting (decentering) of the first two lenses introduces Coma.

Fig. 16b: 20-times "desensitized" interferogram showing the astigmatic wavefront of 540.95 waves PV for a field angle of 25.94 degree.

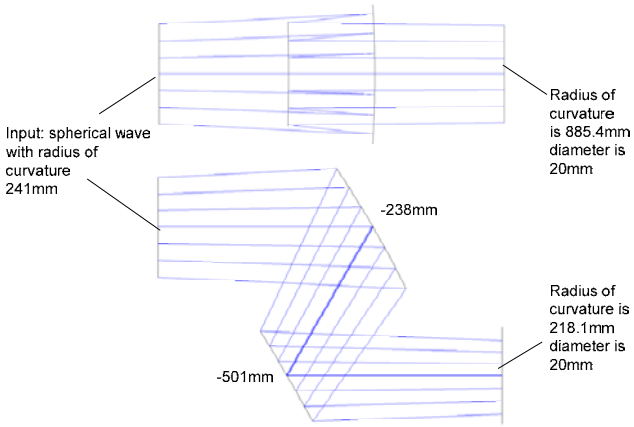

Fig. 17a: A two mirror design as Astigmatism *and* Coma compensator.

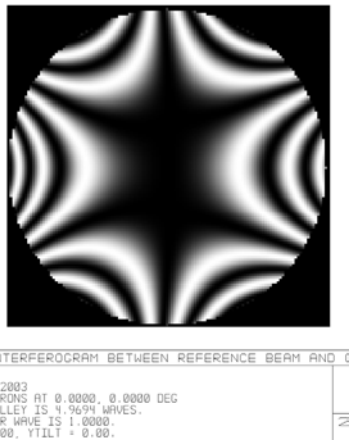

Fig. 17b: Remaining wavefront error for subaperture of 20mm diameter of surface Fig. 15.

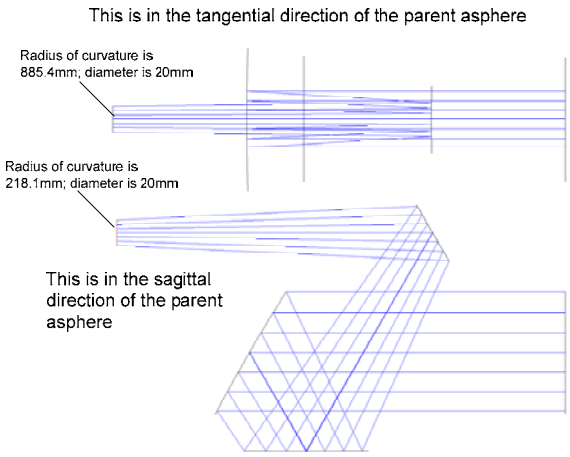

Fig. 18a: A three mirror design as Astigmatism *and* Coma compensator.

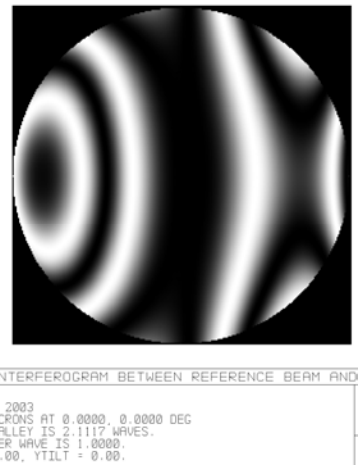

Fig. 18b: Remaining wavefront error for subaperture of 20mm diameter of surf. Fig. 15.

The problem with all these compensators is that their optical effect on the measurement can only be known to a limited uncertainty. When this uncertainty is larger than the errors induced by a direct interferometric measurement of the subaperture, nothing is gained. Coming back to our philosophy, that any additional degree of freedom introduced into the measurement set-up increases the uncertainty of the final result, the compensators could be seen as "removing" *valuable* information from the measurement as compensating exactly these features of the surface, which were characteristic for the aspheric shape in that subaperture, i.e. the amount of Power, Astigmatism and Coma. Taking this standpoint, it is as best a "zero-sum-game".

It will be shown how Zygo's technique reduces the dynamic range in aspheric measurements in-situ to zero, and this without the need for any additional element. For this reason Zygo refrained from patenting the optical compensators for subaperture measurement, developed in 2003. The real worth of these subaperture compensators is when high and mid-spatial frequency content of the surface must be measured, the so called "ripple measurement". Here the high number of pixels on a small part of the surface is the key to low uncertainty and the form of the surface is not aimed to be measured.

7. OPTICAL NULL COMPENSATION

As a consequence to the difficulties and restrictions that are associated with High Dynamic Range Fizeau Interferometry, researchers have thought about adapting the shape of the wavefront used for interferometric measurement to the shape of the aspheric test surface. This can be done either by refractive optics, called null lenses [5,23,27,52], or by diffractive optics, called computer generated holograms (CGH) [3,14,19,25,60]; also the combination of both is possible [7,26]. These elements are placed in the Fizeau cavity, thus being directly included in the optical path difference.

It is immediately clear, that in this case the real difficulty is in providing the compensation device and assuring that it is made correctly. The assumption is that it is easier to test the corrector than the aspheric surface itself. But this technique has another justification: provided that the test set-up including the correction element has been adjusted and qualified, then the test on the test part can be a matter of a minute. This is much faster than for instance the scanning or stitching approaches. As a consequence, it seems the most appealing problem to think about calibration techniques for such test set-ups [12,52].

The most profound and at the same time easiest to perform approach is to use a master part for a calibration measurement; this part has been measured in an absolute manner before, for instance with the method described in section 9 of this paper. In other cases, coordinate measuring machines have been used to measure the master part and fit Zernike functions to the residuals found. Even when the spatial resolution is lost in this step, it is assumed, that the error function in the null-compensation devices is of low spatial frequency only, so the measurement on the same master part can be mathematically corrected by the low-order terms. The mid- and high-spatial frequency errors found in the test with the null-devices are supposed to be correct and are left untouched. Again, the real challenge lies in finding the rotationally symmetric part of the aspheric deviation [27]. The rotationally varying part can be achieved by techniques of separating these parts, the same way, as it is used for spheres and planes. The methods applied for this separation [49,50,51,60] are variations of solving the rotational shearing problem, either exact or approximately. Clearly, this complicates the measurement procedure but opens a possibility for absolute calibration of the set-up for this part of the error, using nothing in addition than the test part itself and a part holder that can be rotated. This is truly an elegant solution!

Another approach proposes to qualify the test-set up by using a dual-wave-front computer-generated hologram [9]. In such a hologram, a spherical as well as an aspheric wavefront are encoded at the same time. The idea here is that the errors found on the reconstructed spherical wavefront, and which can be measured with high accuracy in an absolute sense, can be adapted to the aspheric wavefront as well. Justification: both holograms are written on the same device at the same time. This would be certainly true when the aspheric wavefront would be identical to the spherical calibration wavefront; but as there is necessarily the aspheric departure that differentiates the two, also the errors cannot be identical, at least in higher order. Furthermore the spherical wavefront creates additional unwanted diffraction orders, which is an unpleasant side effect that must be managed somehow.

A similar idea is the basis in Ref.[13], where a refractive null corrector is designed such, that it delivers a spherical wavefront with one wavelength and the wanted aspheric wavefront with another, the test wavelength. In the patent, examples of optics designs are given that can produce a perfect spherical as well as parabolic wavefront, when the wavelength is switched. As with all refractive nulls compared to CGHs, the nice feature is here, that no unwanted diffraction orders, or

digital moiré artifacts are produced that increase the measurement uncertainty due to coherent noise. But some classical compensation arrangements (Offner compensator) place a field lens near an intermediate focus-point and are highly sensitive to producing unpleasant ghosts. [52] In the case of astronomical mirrors, after the disaster with the Hubble telescope, no one would trust a measurement with a single null corrector. The use of a hologram to check the refractive corrector is quite common, but in addition a diamond turned small version of the aspheric test mirror can give additional confidence. [52] Questionable in this case is the influence of the difference in the imaging rays.

Besides the problems of certifying (i.e. measuring) the wavefront encoded in either a null-lens or a CGH, there are a number of other problems that have to be mastered: how to assure the correct alignment between all components. In the case of a null-lens, it is most common to use a plane wavefront as input. Then the degrees of freedom between the main-frame and the null-lens are essentially reduced to two tilts. In the case of a hologram that is placed into a spherical cavity, we have 5 degrees of freedom between the TS lens and the hologram if it is an in-line hologram that has rotational symmetry, or even 6 degrees, if it contains an additional linear carrier-component to facilitate the separation of diffraction orders. Between the aspheric test surface and the null-compensator, we have 5 degrees of freedom of alignment, and these count even more severe than in the case of the measurements discussed in chapter 4, as now steep aspheres must be included in our considerations. Again, without a check of the final result, it is (to my understanding) impossible to get reliable results: as the experience has shown, too much can go wrong! The problem is, that errors can stay unrecognized, and even the argument "I do this all the time and I can repeat my results very well", does not prevent a bug being somewhere hidden. At least, a critical uncertainty analysis including the components as well as all degrees of freedom in alignment of the set-up together with the measured positioning uncertainties is mandatory.

Other problems associated with null lenses and especially with holograms in the beam-path are their imaging properties and conditions. The problems with distortion and defocus have been discussed in chapters 4.2 and 4.4. Now, in the case of a null lens, we have to deal generally with a much larger amount of distortion that can be as high as 20%, which brings the correction to a super-critical part in the uncertainty budget. Even more difficult is the question, what the consequence is of a non-flat image of the test surface on the flat detector and how the image quality either through the null lens or through the CGH will look like (spatial resolution!). These compensation devices fulfill their job by making the imaging of the light source free of aberrations (that is the obvious design criteria, when the aspheric test surface is taken as one component in the image train from the light source). When placed in front of an existing mainframe, there is no degree of freedom left in the optical design to correct this imaging at the same time. In cases, where spatial resolution is critical (telescope mirror to find planets, components for lithographic lenses), the poor imaging properties associated with the compensators can be a real obstacle. Phase-shifts in the coherent imaging train (imaged is the complex amplitude rather than the intensity) can wash out certain spatial frequencies or reverse the phase, i.e. a valley on the part is measured as a hill.

Taking the many error-sources together, the uncertainty associated with measurements with null-correctors becomes large for steep aspheres, i.e. with departures from the best fitting sphere of >1mm, especially when the surface has high NA. Below this value and also for lower NA systems null compensators are a good means for measuring aspheres, especially when a validation with an absolute or quasi-absolute method is possible. The biggest drawback is often the relative high cost, complexity of the set-up and lead-time to produce either a refractive or diffractive null.

The ultimate solution for low measurement uncertainty, stability and ease of use is given by using instead of a TS lens, a TA lens (Transmission Asphere), Ref. [10], that is introduced as the compensation device and the Fizeau-reference at the same time into a reconfigurable interferometer set-up which is calibrated by a absolutely measured master surface, Ref. [11, 12]. Fig. 15 shows as a study with two examples of TA lens designs for two different concave aspheric surfaces; in the first case only spherical surfaces where allowed in the optical corrector design prior to the aspheric Fizeau reference and a matching of the wavefront to the aspheric surface with a residual < $\lambda/10$ was targeted. This led to a very complex design, which would be difficult to be manufactured with the necessary tolerances. In the second case, also one of the inner surfaces of the two-lens Fizeau null-compensator was allowed to be aspheric; now the design is no longer a problem. Keeping the Fizeau cavity as small as possible and using the patented ring source, [41,54] lowers the tolerances on all surfaces of the TA, so that also a commercially competitive result is attained; this is a consequence of the Fizeau.

Whereas refractive null lenses often become very complicated due to the requirement to correct the wavefront to a very small residual which requires a high number of lens elements, which in return lead to non-realistic tolerances, it is an interesting idea to restrict the compensator to a single, spherical lens. This one lens cannot do the job, but it can reduce the aspheric departure to become measurable, using high dynamic range interferometry. Assume that another absolute measurement device is available, that is able to measure the actual aspheric shape of the wavefront that is provided by

the combination of the TS and this single lens, already be mounted to the TS, then a nice set-up results that even allows the measurement of steep aspheres with high throughput. We will describe such an in-situ calibration in the context of Zygo's aspheric measurement machine, the VeriFire Asphere.

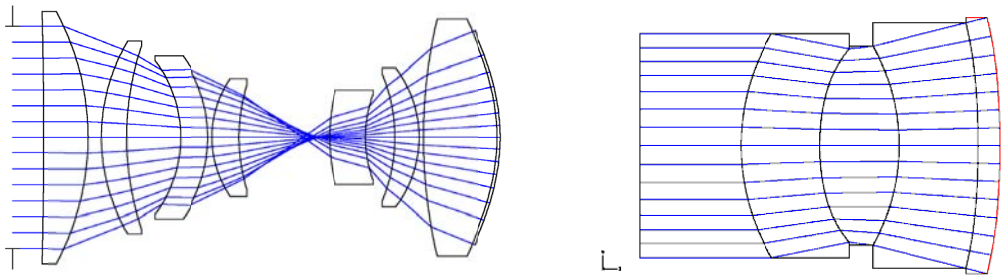

Fig. 19: Two different TA lenses (null-compensator containing the Fizeau reference surface) with a small aspheric Fizeau-cavity. Left: solution with 7 lens elements to achieve the required aspheric wavefront with high NA. Right: only 2 lenses are needed, when also one aspheric surface is allowed in the null-corrector.

8. COORDINATE MEASURING MACHINE (CMM)

Coming back to our considerations of the measurand, chapter 2, it is clear that a CMM [20,35] measures the shape of the aspheric surface against a reference plane: the dynamic range of the problem is 100-times larger than it naturally has to be, just because a non-adapted coordinate system is used . If we replace h^2 by x^2+y^2 in eq. (2) which leads to $z=z(x,y)$ and calculate the partial derivatives of $\partial z(x,y)/\partial x$ as well as $\partial z(x,y)/\partial y$, we see that the values will be generally in the order of magnitude of about 0.5 and that tells us, that all three coordinates show high error-sensitivity, i.e. it is necessary to know all three coordinate values of a point on the surface of the asphere to about the *same* uncertainty. As the measurement forces are always normal to the surface, they change during the measurement in their effect on the three coordinates. In addition, as the measurement is completely sequential we have to fully rely on the accuracy of every single measurement for the final accuracy. In the case of stitching, we could at least at every new position take a very great number of measurements in parallel, and this possibility is used in the stitching software to establish the precise world coordinate system. In CMM, this precision must be built into the machine. Now let us consider some of the difficulties in doing this.

By principle in a CMM the Abbe principle is violated. In addition a spherical, mechanical probe with radius R_{probe} is used to touch the surface, therefore the center of the probe follows a surface which is *parallel* to the measured surface in a constant distance R_{probe}, but only to the accuracy of the roundness errors of the touching probe, see Fig. 16. To be able to calculate the location of the touching point on the surface, the derivatives on the measured surface must be calculated. This can only be defined for a *surface*, not a number of points. This leads to the problem of interpolating a surface between the measured points, and this leads to considerations of the density of the measurement grid, the low-pass filter inherent in the probing sphere with a certain radius. Further considerations and problems are questions of wear, collecting of dirt at the probe, friction between surface and probe, forces in x,y,z direction and dependency of forces from the surface shape. A contradictory requirement is to keep the measurement time short to reduce the sensitivity to thermal drifts, and to keep it long, that the accelerations of masses and the generated dynamic forces and induced changes of the geometry are kept small. This leads to the wish of lightweight construction, structural stiffness by control and altogether a significant engineering challenge. In terms of traceability of the measured result, on a first glance one could argue that we have ideal conditions here: all what must be measured are 3 lengths measurements, and when this is done with a traceable yard stick, as a Laser stabilized to an absorption cell, all is fine and traceable. But as I have briefly mentioned before, many quantities influence the result in a very complex manner. Even when in the attempt to establish a complete measurement uncertainty analysis and a very sophisticated model has been established with the goal to simulate all interactions in a "virtual measuring machine", Ref. [53], it seems more realistic to find out the uncertainty by repeated measurements on a well known test part, like a spherical surface with a similar radius of curvature as the aspheric surface in question. This experiment will not give a complete answer (the result might be too optimistic) since the amount of symmetry in the test part is quite larger in case of the sphere (for instance, 3 rotation directions around the center point do not

change the result), but gives a good starting point that can be complemented by more theoretically based additions to the uncertainty budget.

From a practical point of view, current CMM that are in the range of accuracy needed for optical surfaces are more expensive than interferometric solutions, have higher uncertainties and much longer measurement times. In addition, the number of measured points is much lower, so that the spatial resolution is not comparable and some features, for instance on molded surfaces may remain undetected. Also, the test parts can be destroyed by the touching probe and there is a considerable cost factor for new probes, since they tend to have only a short lifetime.

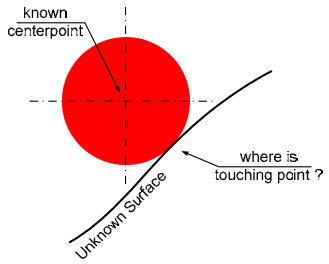

Fig. 20: A CMM measures a number of points that are located on a surface parallel to the measured surface; only a plurality of measured points allows establishing a mathematical model to predict the touch-point.

On the pro side are their high flexibility for different diameters and shapes, including non-symmetrical aspheres. Also, no long preparation is needed and no special tools adapted to the test part like null compensators are needed, so the work can be started immediately.

These machines are a good possibility to verify the result achieved by an optical method due to the independent measurement principle. As a standalone solution for production test, one has to accept the slow throughput, tool-wear and low number of measured points as well as reduced precision (higher noise) compared to interferometry.

9. SCANNING IN A FIZEAU CAVITY WITH RELATIVE PHASE-MEASUREMENTS BETWEEN ZONE AND VERTEX

9.1 The basic idea

As we have seen, the challenges to measure aspheres interferometrically result from the high dynamic range inherent in the measurement problem. A conventional Fizeau interferometer has a limited dynamic range because of the uncertainty with non-common ray-paths in the presence of large slopes. So the goal is to extend the dynamic range of interferometric surface metrology to accommodate strongly-aspheric surfaces while maintaining low uncertainty without the need for any null-compensators.

Our method for asphere metrology [37,38,39,40,41] divides the complete measurement into many (6 to 200, depending on the asphere) sub-measurements of concentric zones, as described in section 5, but we restrict ourselves to gather measurement points only around the center of each zone, where retrace errors are negligible and slope is beyond a predefined value. In addition to the absolute distance of every zone from the center point of the spherical reference surface, we measure the absolute distance also to the apex of the part, so we know the distances R_S and R_V shown in Fig. 21. Because we measure as many quantities as there are unknowns in the problem, every measurement creates an independent result from the other. Stitching of overlapping subapertures is not required to get the surface shape: the ensemble of all results represents directly the surface-deviation in normal direction, greatly improving measurement accuracy when compared to traditional stitching methods. Results are derived directly in the part coordinate system, *(h,z)*. Investigating the tilt in overlapping regions of two zones allows to overcome straightness errors of the scan.

In Fig. 10 we have seen, that an aspheric surface can be understood as the envelope of a family of spheres with different radii. The thick blue lines, arranged along the h-axis with a constant increase Δh, have a height $z(h)$ and define by that points on the asphere. On the other hand, we have normals to the aspheric surface with length R_S, that have intersections

with the symmetry axis (z-axis) in a distance R_v from the apex of the asphere, the shortest distance being R_0. If we draw the red circles, then the envelope is the aspheric surface. So the presentation of the asphere either by $z=z(h)$ or by $R_s=R_s(R_v)$ should in principle be equivalent. We have two variables in both cases, h,z and R_v,R_s and we have a recipe, how to construct the asphere in both cases. The problem is, that the envelope is defined by a continuous change of the parameter R_V and the resulting value $R_s=R_s(R_v)$, but that for one fixed position, as shown in Fig. 21, the angle α of the normal has to be known in addition to compute the Cartesian coordinates h,z of point Q:

$$\begin{pmatrix} h \\ z \end{pmatrix} = \begin{pmatrix} \sin\alpha & 0 \\ -\cos\alpha & 1 \end{pmatrix} \cdot \begin{pmatrix} R_S \\ R_V \end{pmatrix} \tag{17a}$$

$$\begin{pmatrix} R_S \\ R_V \end{pmatrix} = \begin{pmatrix} \frac{1}{\sin\alpha} & 0 \\ \frac{\cos\alpha}{\sin\alpha} & 1 \end{pmatrix} \cdot \begin{pmatrix} h \\ z \end{pmatrix} \tag{17b}$$

Now the question is how to get α. Here we must have two solutions: if we have measured (R_S,R_V), then we also have to measure α or derive it from the measured values (R_S,R_V) in order to be complete and can calculate (h,z) according to (17a), if we want to compute (R_S,R_V) for a given point (h,z), using the design equation (2), then we have to compute α also from the design equation.

$$\alpha = \cos^{-1}\left(\frac{dR_S(R_V)}{dR_V}\right); \qquad \alpha = \tan^{-1}\left(\frac{dz(h)}{dh}\right) \tag{17c}$$

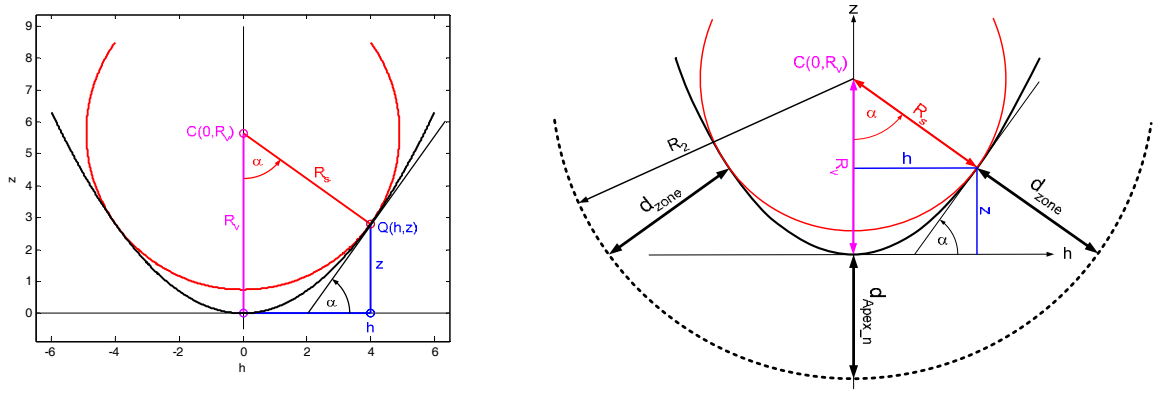

Fig. 21: left: the basic relations between the sagittal radius R_S, the distance R_V of the center point C from the vertex and the Cartesian coordinates h,z. Right hand side: The quantities R_S and R_V are derived from the measurements of the cavity thickness d_{zone} and d_{Apex_n} and the known radius R_2 of the Fizeau surface.

The principle of the measurement of α is shown in the left hand side of Fig. 22. Similar as the differential quotient dz/dh gives a trigonometric function containing α, here the tangents, in the case of the measurement against a sphere we get α from the differential coefficient dR_S/dR_V, but this time the cosine. At a first glance this seems to be a weakness, especially for small values of α, but in practice this is not the case: when α is small, the asphere is close to its center sphere, and therefore the zones are very wide, so R_S does change only very slowly with α. In Fig. 22 left, ΔR_S is the change of the measured phase at a fixed pixel location around the zone, ΔR_V is the change of the phase at the apex; therefore α is measured for a fixed pixel. By this also the magnification M as defined in eq. (13) is found. Practically, there are more possibilities to derive α from the measurement, using the complete scan that is performed to get the surface; for details see e.g. Ref. [13].

As every measurement means comparison, we have only reached our destination when we have made the comparison between the surface as it is and the design shape of the surface, i.e. we have to generate the deviation. Depending on the customer's preference, we can report the deviation in z-direction or in normal direction to the surface. The latter possibility seems more logical to us, as also the fabrication process works normal to the surface, at least in grinding or polishing. The deviation is measured always in normal direction to the design surface, it is the deviation Δn, see Fig. 22 right. The computation of this deviation is not totally trivial: given measured values $R_{S\_measured}$, R_V and α, we now calculate coordinates h and $z(h)$ of point $Q_d(h,z)$ on the design surface; this gives R_{S_design}. Finally, the deviation in normal direction is:

$$\Delta n(h,\theta) = R_{S_{measured}}(h,\theta) - R_{S_{design}}(h) \tag{18}$$

The small difficulty is to compute h of the point $Q_d(h,z)$, as eq. (17a) delivers h of the measured point Q_m. But we can use an iterative solution with the following set of equations:

$$h_{n+1} = \frac{(R_V + h_n \cdot z'(h_n) - z(h_n)) \cdot \tan\alpha}{1 + z'(h_n) \cdot \tan\alpha}; \qquad z_{n+1} = z(h_{n+1}) \tag{19a}$$

Finally:
$$R_{S_{design}} = \frac{h_{n+1}}{\sin\alpha} \tag{19b}$$

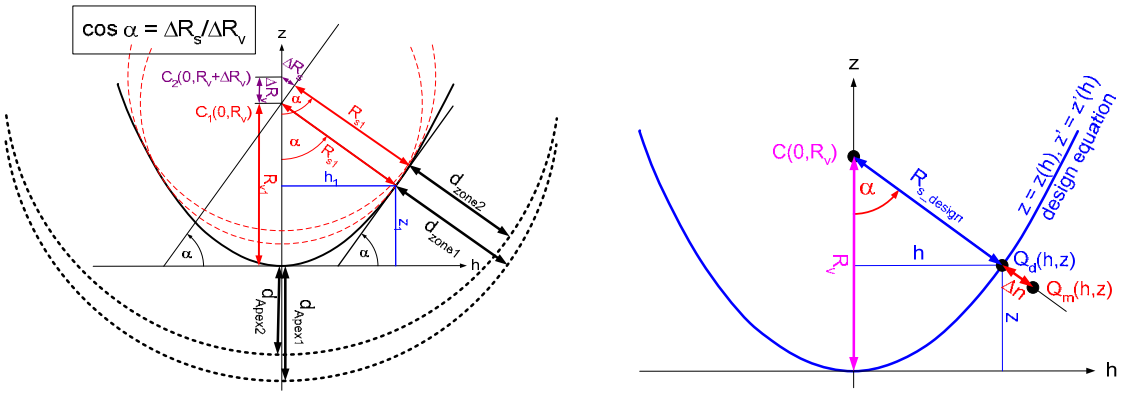

Fig. 22. Left: the aperture angle at the zone is derived from the phase-differences of two measurements, where the test surface is moved by ΔR_V; please notice that α is constant if the same pixel is observed. Right: the surface departure from design is measured in normal direction; see text.

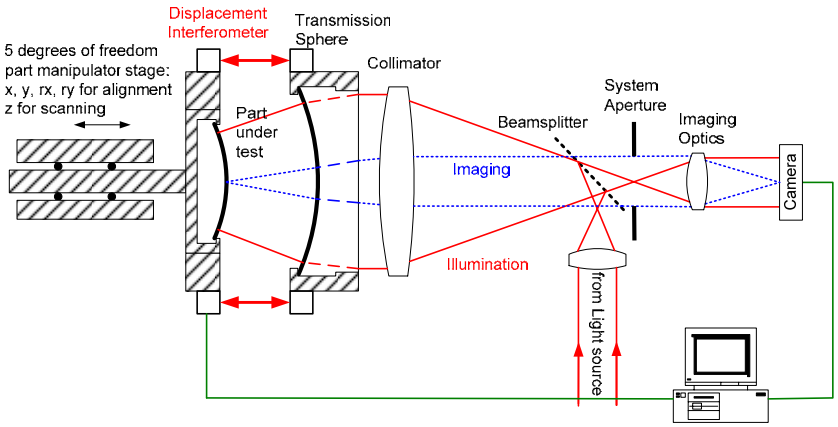

Fig. 23: Schematic sketch of the complete machine, including TS lens and mainframe. A part manipulator stage is shown that performs the scan after alignment of the optical axis of the asphere to the scan-direction. The purpose of the displacement interferometers will be explained in 9.2.

This is the basic principle, how by simultaneously measuring the cavity distances d_{zone} and d_{apex} the departure $\Delta n(h,\theta)$ can be computed finally with very high precision and free of all the error sources discussed before, as retrace errors, errors induced by defocus or errors due to distortion. As the results are all based on nothing but *relative* lengths measurements on two different locations on *two solid bodies*, it is clear that the process is very insensitive to outer disturbances, like drift. If for instance the z-position of the part is changed by drift, this does not harm, since it is measured. Also, the measured cavity thicknesses at the apex, d_{apex} and at the zone, d_{zone} stem from the same phase-measurement on the same detector, i.e. they are exactly simultaneous. But the most remarkable fact is that we get the result directly in the object

coordinates of the part. This is a unique feature that is unparalleled in all other techniques and new in interferometry altogether. So the difficult problem of registration between detector coordinate system and part coordinate system is avoided, and it would even be possible to change the magnification between different zones. Distortion has no effect on the precision of the measurement result, so a calibration is not needed. And I hope that it was made clear, that the results on the zones are independent, so stitching is not needed to bring them together. When due to practical reasons of measurement speed wider zones are used for the data evaluation (area around the point *Q*), then results from overlapping areas can simply be averaged, using appropriate weights considering the increasing uncertainty with increasing slope.

9.2 Refinements

So far we have described the principle, which, due to the rotational symmetry of the aspheres, can be discussed as a two-dimensional problem. As the third dimension we use the azimuthal angle θ, and so far there was no need to deal with θ, as nothing depended on this variable. In real world, this is quite different! Now we have to cope with problems like deviation of the measured surface from the design by amounts as large as several µm, astigmatism in the surface, non-ideal mechanical behavior of the scanning device, special aspheric shapes that are difficult to measure, for instance multiple zones, and more. I will describe now briefly only a few of the additional problems that arose in the 3D case and had to be solved.

The scan distance is given by the change of the quantity R_V for $0 \le h \le h_{max}$. For $h=0$ it is $R_V=R_0$, i.e. we always start the scan at the home position, where the center point of the Fizeau reference surface coincides with the center of the apex sphere. For some calculations, it is more convenient to work directly with the scan movement $v=R_V-R_0$, than with R_V, and similar with the height difference between apex and zone on the aspheric surface, which we call $p=R_V-R_S$. We see that our most valuable measurand is p, as this is the characteristic of the asphere, but also v is important, as the independent variable. Using p,v, as well as $p'=dp/dv$ as the set of 3 variables, we can reformulate the equations (17):

$$v = z - R_0 + \frac{h}{z'} \qquad (20a) \qquad\qquad h = (R_0 + v - p)\sqrt{p'(2-p')} \qquad (20b)$$

$$p = z + \frac{1-\sqrt{1+z'}}{z'} \cdot h \qquad (21a) \qquad\qquad z = p + (R_0 + v - p) \cdot p' \qquad (21b)$$

$$\frac{dp}{dv} = p' = 1 - \frac{1}{\sqrt{1+z'^2}} \qquad (22a) \qquad\qquad \frac{dz}{dh} = z' = \frac{\sqrt{p'(2-p')}}{1-p'} \qquad (22b)$$

In these coordinates, the arrangement can be shown as in Fig. 24, which also shows the point $E(h_e,z_e)$ on the evolute of the asphere. The coordinates h_e, z_e as well as the radius R_e of the evolute are readily computed using eq. (2):

$$h_e = h - \frac{z'}{z''}(1+z'^2) = -\frac{\sqrt{(p'(2-p'))^3}}{p''} \qquad (23a)$$

$$z_e = z - \frac{1}{z''}(1+z'^2) = \frac{(2-3p'+p'^2)p'}{p''} + R_0 + v \qquad (23b)$$

$$R_e = \frac{\sqrt{(1+z'^2)^3}}{z''} = \frac{(2-p')p'}{p''} + R_0 + v - p \qquad (23c)$$

$$\Delta = \frac{\eta^2 |hz''' - z' - z'^3|}{8h(1+z'^2)^3} \qquad (23d)$$

Values R_e are needed to predict the width η of the zone given a certain values for the astigmatic deviation Δ, and to decide on well suited values v_1 and v_2 for an initial alignment of the aspheric surface parallel to the scan direction. As we have 4 degrees of freedom for alignment, lateral shifts Δx, Δy as well as rotations r_x and r_y (tip and tilt) around the axis, we need 2 measurements of the x-tilt and y-tilt components in two different zones (at different values h_1 and h_2) to solve the alignment problem. The selection of the zones depends on the location of the evolute points E_1 and E_2. Our software selects the best suited values and performs an auto-alignment.

After auto-alignment, the measurement starts by moving the apex of the surface to cat's eye position, where the center M of the reference surface (see Fig. 24) coincides with the vertex S_A of the aspheric surface. From this point on, the stage travels the commanded distance R_0 back to the home position; here the distance measuring interferometers are set to zero. Then the scan starts in m-predefined steps according to a test plan, that the software has automatically generated

analyzing the aspheric equation. To keep the measurement time as short as possible, the number *m* is minimized; in cases where the actual test part deviates much from the design equation, it could turn out that the value chosen for *m* must be increased; this is then an operator interaction. The width η of the *m*-zones, where measurement data are collected and used to derive the surface deviation from design, see Fig. 24, is limited by the allowed surface slope; this can be set by the operator and is an important parameter for *m*. As a standard value, we set the limit at 1/10 Nyquist; here the errors discussed in chapter 4 are still in a reasonable small range and the zones wide enough for phase-unwrapping.

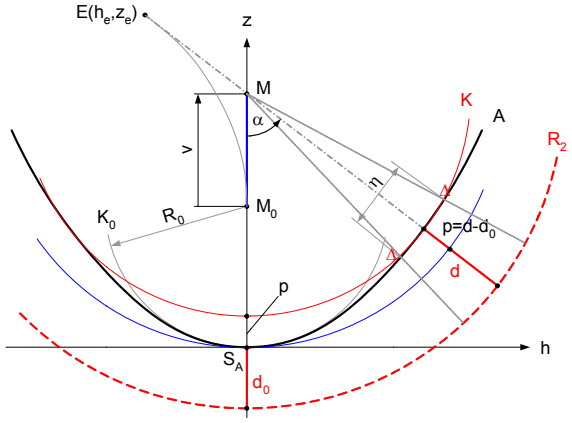

Fig. 24: A different description of the basic configuration, when using eqs. (20), (21), (22)

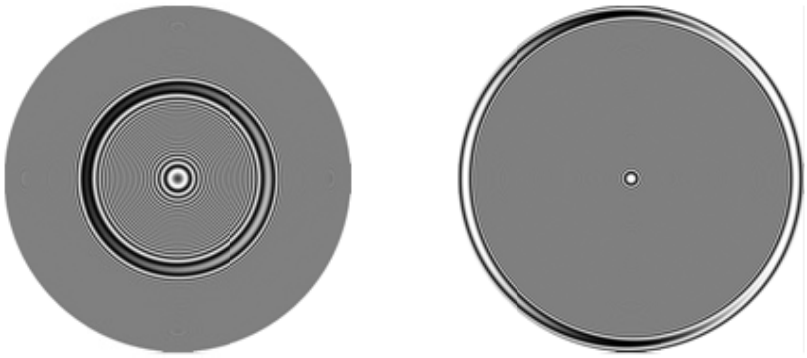

Fig 25: Zones chosen for auto-alignment; in this example, the chosen scan positions have been v_1=0.861 and v_2=2.443, so Δv=1.582. The tilt still visible in the zones is greatly exaggerated for clarity; in reality, after the alignment procedure is finished, no visible non-symmetry is left.

The easiest realization of the machine would be possible, if the interferometric distance measurements d_0 and d, on the vertex and the zone, see Fig. 24, would be absolute, i.e. not ambiguous by $\lambda/2$ due to the temporal coherence of the HeNe-laser and the $mod(\varphi,2\pi)$ characteristic of phase-measurement. We solve this problem by using the displacement interferometers, shown in Fig. 23, as "helpers" to get the correct interference order back after a shift Δv of the stage; this is without any problem, and the final phase-value is absolute, where the distance measuring interferometers have assured that the integer part is correct, the Fizeau phase-measurement has delivered the fringe fraction with highest precision. For the prediction of $\Delta p(\Delta v)$, which is a much smaller value than Δv, we also could perform a tracking procedure predicting the next value from the design equation, but there are even better possibilities. As we work with overlapping regions, we always see the same region on two successive zones; this can be used to predict the (integer) order number for Δp, when p is expressed in fringe orders. It must be emphasized, that the accuracy of the distance measuring interferometers drops out in the final result, as long as the measurement uncertainty allows predicting the fringe order number, and this is for sure the case if the uncertainty is smaller than 40nm; the actual accuracy is much better. The uncertainty of the asphere measurement depends on other factors and is given in the specifications. [41]

9.3 Measurement of intrinsic Coma

There is another interesting aspect in the realization of the principle: this has to do with the degrees of freedom and their consequences for the final measurement result of this measurement principle. As we have discussed, degrees of freedom in adjustment make us blind for the response functions they create. Now, in our measurement we have to shift the test part such, that the straight symmetry axis of the aspheric surface to be tested coincides in every scan position with the center point of the reference surface, see the cartoons in Fig. 26 left and center. If our shift was perfect, then all the zones will show no tilt fringes; if we see tilt fringes, they must be the consequence of a non-perfect shift. So, if we make the assumption of an a priori *straight* rotation axis of the aspheric surface, then our life is easy: we could either correct tip/tilt of the stage at every scan position, thus bringing the symmetry axis back to the center point in space, or, even simpler, subtract the tilt terms by software with exactly the same effect. Doing either the first or second approach is very well justified, since most aspheric surfaces really possess an almost perfectly straight symmetry axis, for instance when they are produced by diamond turning. But it is still bothering, that we would not measure correctly the surface, if its symmetry axis was not straight. As we did not want to bother ourselves nor our customers, we thought about solutions. There are several, and we will explain them briefly.

First we have to clarify, what a non-straight symmetry axis of the part means for the surface-departure in normal direction to the surface. Let us assume a zone with a diameter $2h$ and sagittal radius $R_S=R_0+v-p$, see Fig. 26 right and Fig. 24. Then a lateral deviation Δh of the symmetry axis (shown in the plane of the drawing, but might be at an angle θ) causes the measured cavity thickness change by c_p at one side and $-c_p$ on the opposite side. Thus the equivalent error in normal direction is:

$$c_p(h) = \Delta h \cdot \sin\alpha = \Delta h(v)\,\frac{h}{R_0+v-p} \tag{24}$$

In eq. (23) v and p depend on h and can be taken from the design surface. In the three dimensional case, introducing the azimuthal coordinate θ, we have $\Delta h(v,\theta)$ and therefore $c_p(h,\theta)$ and can formulate:

$$C(h,\theta) = a(h)\sin\theta + b(h)\cos\theta \tag{25}$$

$$a(h) = \frac{1}{2\pi}\int_0^{2\pi} c_p(h,\theta)\sin\theta\cdot d\theta \tag{26a}$$

$$b(h) = \frac{1}{2\pi}\int_0^{2\pi} c_p(h,\theta)\cos\theta\cdot d\theta \tag{26b}$$

$C(h,\theta)$ is the *intrinsic* Coma that a surface might contain. The amplitude and azimuthal location are given by:

$$d(h) = \sqrt{a(h)^2 + b(h)^2} \tag{27a}$$

$$\theta_0 = \tan^{-1}(a(h), b(h)) \tag{27b}$$

Note that due to the Fourier integral (26) the coefficients a and b defining intrinsic Coma are derived as an *average* tilt; these values are smaller than a local bump or hill that the surface on a concentric circle might have. Note further, that Coma is an odd-function: rotating the function by 180 degrees changes the sign. In addition, the function is of low spatial frequency with respect to θ. The spatial frequency-content in the functions $a(h)$ and $b(h)$ is scaled with the slowly varying numerical aperture $\sin\alpha$ but depends mainly on the spatial frequency in Δh, and this will largely depend on the production procedure. If this is polishing, the tool size will play an important role. But it can be assumed, that $a(h)$ and $b(h)$ should be small quantities. From this derivation of intrinsic Coma it is also clear, that its effect on the measurement is the same as a non-straight scan axis or a tilt of the part during scan.

The easiest solution from the standpoint of the software would be to make the mechanical scan-device better than the uncertainty that should be reported for the intrinsic coma. But this would lead to a very expensive mechanical device; the relationship between for instance the lateral shift Δh of the measured part (looking for a moment only at the straightness of the scan device) and the induced tilt on the surface is shown in the Fig. 26, right. The measured value c_p as a function of Δh, as given by (24) shows, that Δh and c_p have similar magnitude, so to keep c_p small, the straightness device should have optical quality, i.e. deviations of nm rather that µm. For a commercially viable product, the cost would be too high.

The second consideration is if we could not afford a mechanical guidance that is straight enough, could we make one that is repeatable to the desired accuracy? If this would be the case, then we could do two measurements and rotate the part in between by 180 degrees. When the result of the second measurement is rotated back by software, and both results aver-

aged, the influence of the guidance would drop out (well known principle of reversal). It is interesting to notice, that this solution would still work through many repeated measurements, if there is a random component to the movement of the stage, in addition to the systematic part: the random component would reduce with the square root of measurements. But we did not favor this solution, because it would increase the measurement time at least by 2.

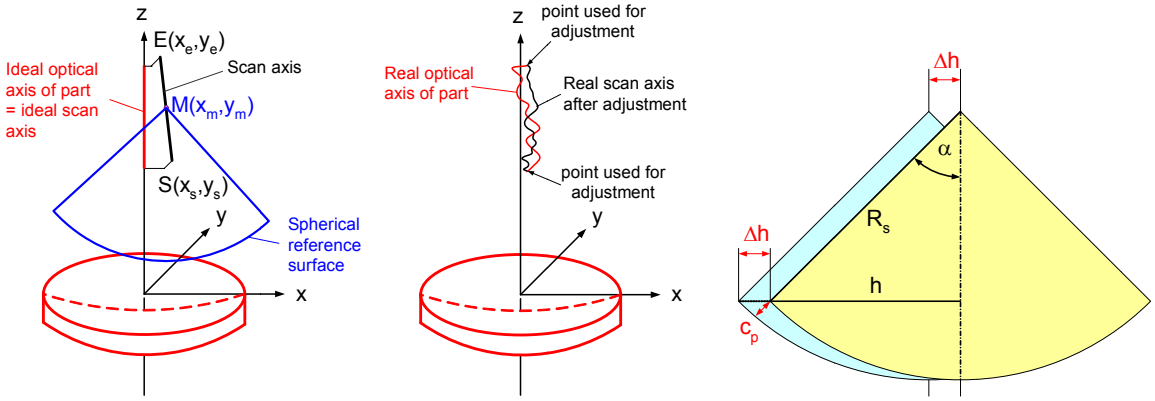

Fig 26: Left: ideally straight optical axis and ideally straight scan axis, but misalignment of axis relative to each other. The lateral offsets are x_s,y_s at start point of scan and x_e,y_e at end point of scan with length Δv. Center: real non-straight optical axis of asphere (greatly exaggerated) and real", non-straight mechanical scan axis (greatly exaggerated) with ideal alignment at end-points of scan. Right: relationship between lateral offset Δh of center-point of Fizeau reference surface and optical axis of aspheric surface with measured height-error c_p at zone with radius h and sagittal radius R_S.

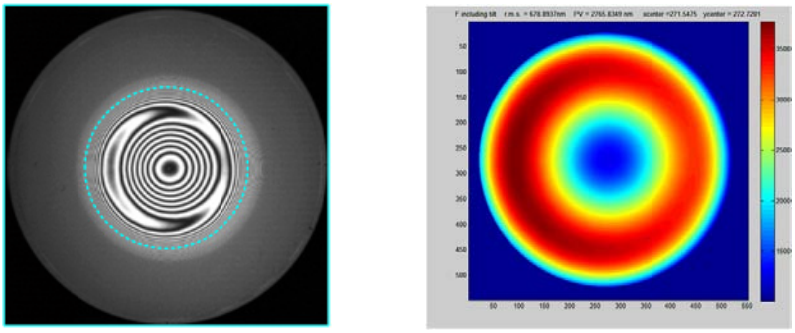

Fig. 27: left: interferogram of an aspheric surface measured near the home position; some misalignment is left; right: height map of the measurement to the left; design asphere not subtracted.

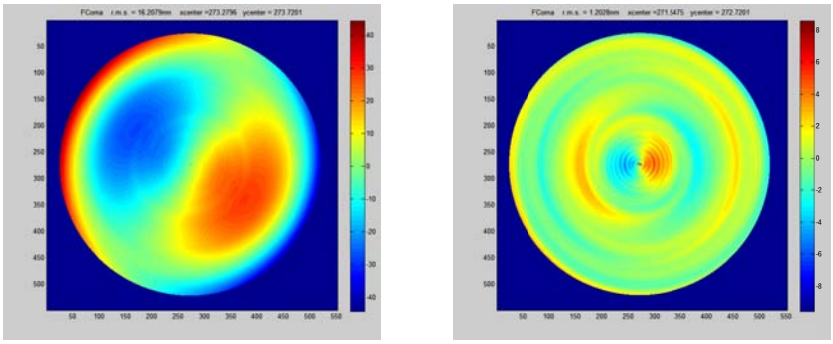

Fig. 28: left: Alignment Coma contained in the height map of Fig. 27 right. Alignment Coma stems purely from the definition of the center of the coordinate system, it is NOT a surface feature. Right: Intrinsic Coma contained in the height map of Fig. 27 right. This is the very small residual that cannot be removed by the choice of the coordinate system. Compare the r.m.s values of the Figures!

Finally, we were able to find a solution that is purely by software: the key is, that the measured zones have a finite width, and that we make measurements where two adjacent zones have an overlap of 1/2 the width of every zone. In this common region, the part has the same intrinsic Coma: if we see a change, this must be due to the stage. As the coefficients *a(h)* and *b(h)* are computed with extremely good precision, this procedure is very stable and gives repeatable results.

9.4 Measurement results and correlation study

The technique has been used for the development of a commercial measurement machine, the Zygo VeriFire Asphere, Ref. [40,41] , as shown in Fig. 29.

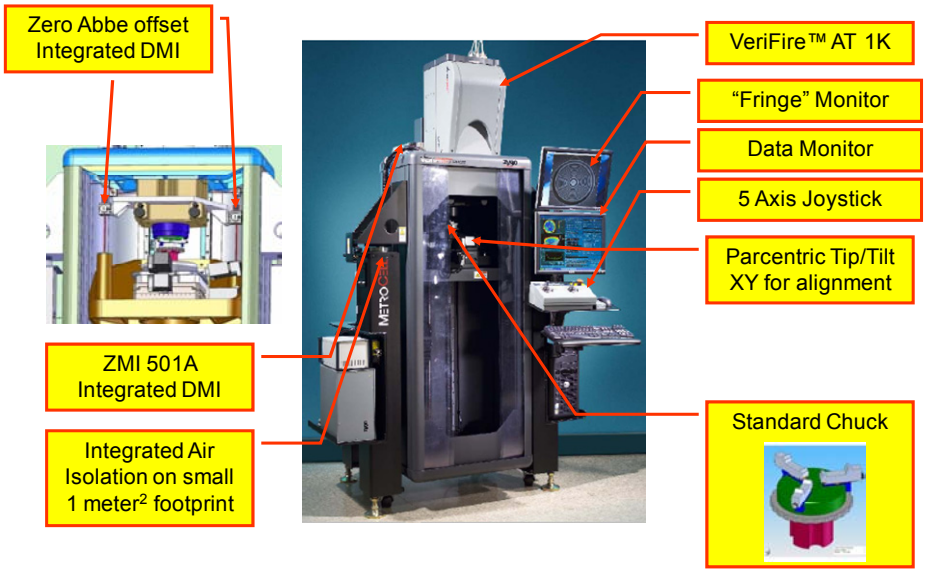

Fig. 29: Zygo VeriFire Asphere

Goals for the development were ease of use (automated alignment) and fast measurement time, as well as flexibility. The set-up measures a wide range of aspheric surfaces in about 5 min measurement time including alignment [41]. To verify our theoretical considerations and error budget by experiment, we performed a correlation study, Ref. [61], using a diamond turned parabolic artifact as the test part that could be measured on the VeriFire Asphere system as well as in a null-configuration, where a plane wavefront is transformed into a spherical wavefront converging to the focus point. Fig. 30 shows symbolically the rays in both set-ups. Fig. 31 shows results for both, the measurement taken by the VeriFire Asphere as well as by the conventional set-up with a spherical auto-collimation mirror.

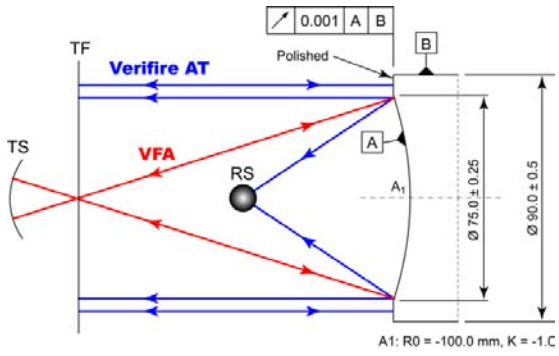

Fig. 30: Two measurements taken on the parabolic artifact. Blue: conventional null-test with a reference sphere RS as auto collimation mirror and a transmission flat TF as reference. Red: one scan position with zone (= normal incidence) at the edge of the parabola; reference is a transmission sphere TS.

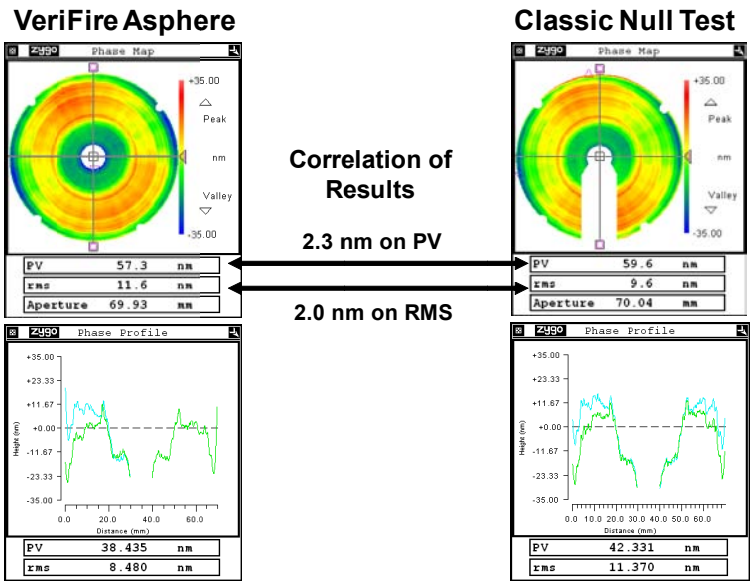

Fig. 31: Results of both measurements. It should be noted, that in the case of the conventional null test the focus has been set to the RS (auto-collimation sphere), i.e. the detector is located between two defocused images of the surface under test. In addition, the angles of incidence on to the surface change in the classical test, i.e. the sensitivity for surface errors changes too.

The measurement results agreed to the extent that can be expected, considering not only the errors associated with the additional surfaces TF and RS in the case of the null-test configuration and TS in the VeriFire Asphere measurement, but also the optically relevant differences in the two set-ups. In particular, the imaging of the surface under test onto the detector is problematic in the conventional null test, because two images of the test surface, separated by a considerable z-distance, exist. We have chosen to set the detector between both images, to minimize the defocus-effect of both. Nevertheless it could be observed on the profile traces (see Fig. 31 right) that some high frequency information was diminished.

Fig. 32 shows some more typical measurement results, which were from different catalogue aspheres.

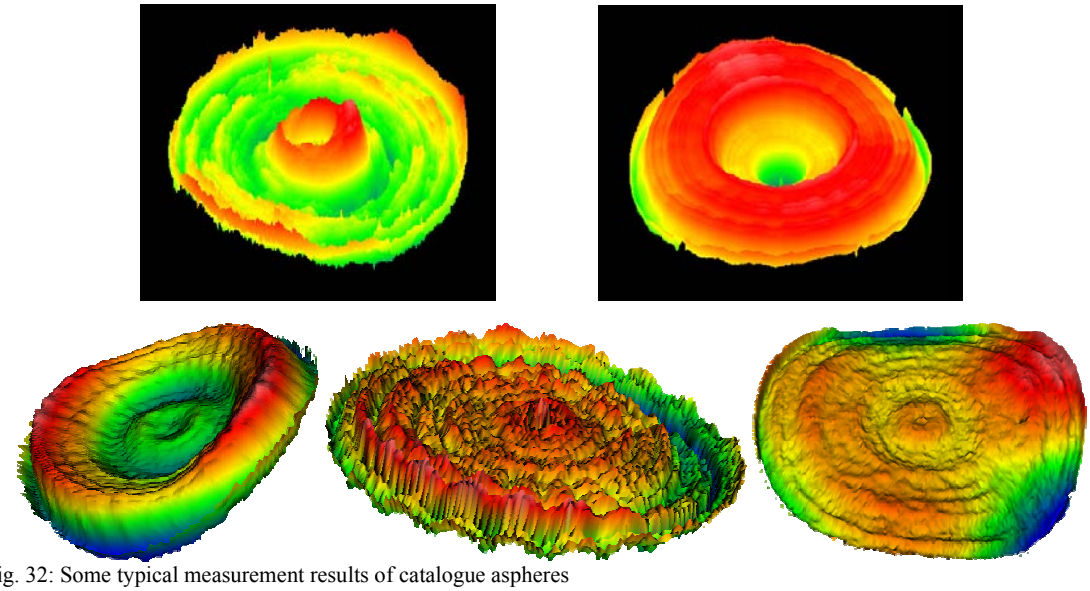

Fig. 32: Some typical measurement results of catalogue aspheres

9.5 Summary

The paper starts with basic considerations of the dynamic range inherent in the task to measure steep aspheric surfaces. Then different methods to deal with this high dynamic range are discussed briefly together with their dominant error sources. These are direct interferometric measurements in a Fizeau set-up, zonal stitching techniques as well as general stitching techniques with and without partial optical compensation. Next we discuss compensation techniques using either null lenses or holograms and emphasize the need for verification and calibration of these devices. Finally measurements using a coordinate measuring machine and a mechanical probe are discussed briefly. Then we present our VeriFire Asphere technique in more detail.

In the VeriFire Asphere System multiple measurements are performed to reduce the dynamic range of the problem, but this time it can be reduced to zero. The problems usually associated with multiple measurements, i.e. dealing with different coordinate systems, are avoided, since the partial results are all collected in one and the same coordinate system, and this is the coordinate system of the part under test, not the interferometer (detector) coordinate system. Therefore also the error source of magnification and distortion (mapping errors) is removed by principle. The other problem discussed was that of degrees of freedom due to multiple part positions; in this method where we measure distances of the surface against the center point of the spherical reference surface which is fixed in space, there are 3 degrees of freedom in every scan position. The *z*-position is measured interferometrically, leaving only *x,y* as degrees of freedom; these can be derived from the measured global tip/tilt component in every zone. For the essential quantity, i.e. the aspheric profile, only the piston term is needed, not tip/tilt, so the latter terms are only important for the rotational varying component of the aspheric surface. Even without measuring the straightness (and angular variations) of the scan, these tip/tilt components can be derived when we use tip/tilt information from overlapping regions. This way, even intrinsic Coma of the surface can be reported. In addition, the measurement delivers the base radius R_0 of the aspheric surface. As the instrument can measure aspheres with departures from sphere of up to 1mm and departures from design up to 10µm, is very fast (≈ five minutes), is as precise as we expect from Fizeau interferometry with nulled fringes, is absolute if we use a beforehand absolutely calibrated reference surface, and does not need any tool like null-corrector that is expensive and needs lead time, it is ideally suited for measurement in production. Unparalleled high dynamic range, low measurement uncertainty and large number of measured points have helped customers to identity features in their aspheres that have been overlooked with other methods and clearly uncovered problems associated with their production method. Their satisfaction is the real gratification for hard work!

But the potential of this method goes beyond what is realized today, and it is especially valuable for the absolute measurement of calibration masters used in another set-up with partial or null-compensation to correct the result, or is used directly to measure the aspheric shape of a wavefront delivered by a corrector. In the latter case, the role of the spherical reference surface and the aspheric part, that is scanned, are reversed: now an absolutely calibrated spherical mirror is used for the scan.

ACKNOWLEDGEMENTS

My colleagues at Zygo, Thomas Dresel and Michael Turzhitsky have in two independent projects done exceptional contributions helping to turn an idea into a real-world metrological solution. [39,40,41] I am grateful to them for their ideas and great professional excellence for writing and testing software to conquer uncounted small as well as large practical difficulties and finding the best solution, as well as for many discussions, that were enrichments to my own understanding of the matter and contained many valuable challenges. Without saying, software just by itself does not do anything useful: a whole team of engineers and marketing people was busy to make this a superior metrology tool. I want to express my special thanks to David Stephenson, Sue Lathan, Daniel Sykora, Robert Smythe, Michael Pickett, Karta Khalsa and John Cordero.

REFERENCES

[1] http://imaging.nikon.com/products/imaging/technology/scene/25/index.htm
[2] http://www.canon.com/technology/canon_tech/explanation/aspherical.html

[3] Dörband, B.: "Analyse optischer Systeme," Chapter 5.1.5., Dissertationsschrift, Institute for Technical Optics, Stuttgart, (1986).
[4] Liu, Ying-Moh, Lawrence, G.N., and Koliopoulos, Ch.: "Subaperture testing of aspheres with annular zones," Appl. Opt. 27, 4504-4513 (1988).
[5] Malacara, D.: *Optical Shop Testing, 2nd Ed*., "Null Tests Using Compensators," Wiley Interscience, (1992).
[6] Melozzi, M., Pezzati, L., Mazzoni, A.: "Testing aspheric surfaces using multiple annular interferograms," Opt. Eng., **32**, p 1073, (1993).
[7] Adachi, I.P.: "General aspherical surface optical testing device," US Patent 5,245,402 (1993).
[8] Huang, J.-J., Lin, T.: "Interferometric method for optical testing an object with an aspheric surface," US Patent, 5,625,454 (1997).
[9] Beyerlein, M., Lindlein, N., and Schwider, J.: "Dual-wave-front computer-generated holograms for quasi-absolute testing of aspherics," Appl. Opt., 41, 2440 - 2447, (2002).
[10] Zanoni, C.A.: "Apparatus and method for measuring aspherical optical surfaces and wavefronts," US Patent 6771375 (2004).
[11] Küchel, M.: "Reconfigurable interferometer system," US Patent 6943896, (2004).
[12] Evans, Ch., Küchel, M.: "Rapid in-situ mastering of an aspheric Fizeau," US Patent 6714308, (2004).
[13] Küchel, M., "Dispersive null-optics for aspheric surface and wavefront metrology," US Patent 6717679 (2004).
[14] Simon, F., G. Khan, K. Mantel, N. Lindlein, and J. Schwider: "Quasi-absolute measurement of aspheres with a combined diffractive optical element as reference," Appl. Opt., **45**, 8606-8612, (2006).
[15] Wang, X., Wang, L., Yin, L., Zhang, B., Fan, D., Zhang, X.: "Measurement of large aspheric surfaces by annular subaperture stitching interferometry," Chinese Optics Letters, Vol. **3**, 645-647 (2007).
[16] Hou, X., Wu, F., Yang, L., Chen, Q.: "Experimental study on measurement of aspheric surface shape with complementary annular subaperture interferometric method," Optics Express, Vol. **15**, 12890-12899 (2007).
[17] Chen, S., Li, S., Dai, Y., Ding, L., and Zeng S.: "Experimental study on subaperture testing with iterative stitching algorithm," Optics Express, Vol. **16**, pp. 4760-4765 (2008).
[18] Garbusi, E., Pruss, Ch. and Osten, W.: " Interferometer for precise and flexible asphere testing," Optics Letters, Vol. **33**, 2973-2975 (2008).
[19] Fercher, A.F.: "Computer-generated holograms for testing optical elements: error analysis and error compensation," Opt. Acta **23,** 347–365, (1976).
[20] Becker, K. and E. Heynacher: "M400 – a Coordinate Measuring Machine with 10nm Resolution," Proc. SPIE 802, pp. 209-216, (1987).
[21] Kitabayashi, J.M., Kanoh, T.: "Device for optically measuring aspheric surface," US Patent 4,743,117 (1988).
[22] Beckstette, K.: "Fabrication of X-Ray Optics," Proc. SPIE 1140, R. Benattar, ed., pp. 316-329 (1989).
[23] Küchel, M., Wiedmann, W.: "In-process metrology for large astronomical mirrors," In: Advanced optical manufacturing and testing; Proc. SPIE A92-17451 05-74, pp. 280-294 (1990).
[24] Glenn, P.: "Lambda-over-one-thousand Metrology Results for Steep Aspheres using a Curvature Profiling Technique," Proc. SPIE 1531, p. 54, (1991).
[25] Burge, J.H. and Anderson, D.S.: "Full-Aperture interferometric test of convex secondary mirrors using holographic test plates," Proc. SPIE 2199, pp 181-192, (1994).
[26] Burge, J. H., Anderson, D.S.: "System and method for interferometric measurement of aspheric surfaces utilizing test plate provided with computer-generated hologram", US Patent, 5,737,079 (1998)
[27] Schillke, F.: "Critical aspects on testing aspheres in interferometric setups," Proceedings Optical Fabrication and Testing, Europto Series Vol. 3739, pp317-324, (1999).
[28] Sommargren, G.E., Phillion, D.W., Johnson, M.A., Nguyen, N.Q., Barty, A., Snell, F.J., Dillon, D.R. and Bradshelher, L.S.: "100-picometer interferometry for EUVL," in Emerging Lithographic Technologies VI, Pts 1 and 2, Proc. SPIE 4688, pp. 316-328, (2002).
[29] Tronolone, M.J., Fleig, J.F., Huang, C.H., Bruning, J.H.: "Method of Testing Aspherical Optical surfaces with an Interferometer," U.S. Patent 5,416,586.
[30] Griesmann, U., Soons, J., Wang, Q. and DeBra, D.: "Measuring Form and Radius of Spheres with Interferometry," CIRP Annals - Manufacturing Technology, Vol. 53, pp. 451-454, (2004).
[31] Assoufid, L. Bray, M., Quin, J., Shu, D.: "3-D surface profile measurements of large x-ray synchrotron radiation mirrors using stitching interferometry;" Technical Report, DE2002-801583; http://www.ipd.anl.gov/anlpubs/2002/09/44233.pdf
[32] Greivenkamp John E.: "Sub-Nyquist interferometry," Appl. Opt. **26**, 5245-5258 (1987).

[33] Arnold, S.M., Kestner, R.: "Verification and Certification of CGH Aspheric Nulls," Proc. SPIE 2536, pp. 117-126 (1995).
[34] Fleig, J., Dumas, P., Murphy, P.E. and Forbes, G.W.: "An automated subaperture stitching interferometer workstation for spherical and aspherical surfaces," Proc. SPIE 5188, 296-307 (2003).
[35] Tsutsumi, H., Yoshizumi, K., Takeuchi, H.: "Ultrahighly accurate 3D profilometer," Proc. SPIE, Vol. 5638, 387-394 (2005).
[36] Blümel, Th., Bosse, M.: "Interferometric Asphere Testing in a Spherical Test Setup," Detectors and Associated Signal Processing II. Edited by Chatard, Jean-Pierre; Dennis, Peter N. J. Proceedings of the SPIE, Volume 5965, pp. 351-358 (2005).
[37] Küchel, M. US Patent No. 6781700, 6972849, 6879402.
[38] Küchel, M. "Absolute Measurement of Rotationally Symmetrical Aspheric Surfaces," in *Optical Fabrication and Testing 2006* (OSA), OTFuB5.
[39] Küchel, M.F.: "Interferometric Measurement of Rotationally Symmetric Aspheric Surfaces," Optifab (2007) http://www.zygo.com/library/papers/proc_TD04-25.pdf
[40] Smythe, R.: "Asphere interferometry powers precision lens manufacturing," LaserFocusWorld, October (2006).
[41] http://www.zygo.com/met/interferometers/verifire/at/verifire_at_specs.pdf
http://www.zygo.com/met/interferometers/verifire/asphere/verifire_asphere_spec.pdf
[42] Murphy, P., Fleig, J., Forbes, G., et al.: "Subaperture stitching interferometry for testing mild aspheres," Proc. SPIE 6293, 62930J-1-62930J-10 (2006).
[43] http://www.engsynthesis.com/pdfs/intellium_asphere_overview.pdf Engineering Synthesis Design, Inc.; Copyright (2009). Rev 1.2
[44] Dörband, B. and H. J. Tiziani: "Testing aspheric surfaces with computer-generated holograms: analysis of adjustment and shape errors," Appl. Optics **24** (16), 2604-2611, (1985).
[45] Evans, C.J.: "Compensation for Errors Introduced by Nonzero Fringe Densities in Phase-Measuring Interferometers," Annals of the CIRP Vol. 42/1, 577-580 (1993).
[46] http://de.wikipedia.org/wiki/Evolute
[47] Murphy, P.E., Brown, Th.G., and Moore, D.T.: "Interference imaging for aspheric surface testing," Appl. Opt. **39**, 2122-2129, (2000).
[48] Forbes, G.W.: "Shape specification for axially symmetric optical surfaces," Optics Express, Vol. **15**, Iss. 8 – April 16, 2007, pp. 521-5226.
[49] Evans, C.J., and Kestner, R. N.: "Test optics error removal," Appl. Opt. **35**, 1015–1021 (1996).
[50] Freischlad, K. R.: "Absolute interferometric testing based on reconstruction of rotational shear," Appl. Opt. **40**, 1637–1648 (2001).
[51] Küchel, M.F.: "A new approach to solve the three flat problem," Optik (Jena) **112**, 381–391 (2001).
[52] Sasián, J. M., Lerner, S.A., Burge, J.H. and Martin H.M.: "Design, tolerancing, and certification of a null corrector to test 8.4 meter mirrors," SPIE Vol. 3739 (1999).
[53] Schwenke, H.: "Abschätzung von Messunsicherheiten durch Simulation an Beispielen aus der Fertigungsmesstechnik," TU Chemitz, Diss., (1999).
[54] Küchel, M.: "Spatial Coherence in Interferometry," http://www.zygo.com/library/papers/optatec2004.pdf
[55] Malacara D., Malacara Z.: "Handbook of Lens Design," Chapter 2, Marcel Dekker, (1994).
[56] Evans, Ch. J., Küchel, Ch. G., Parks, R. E. and Kuhn, W., P.: "Adaptive nulls for testing off-axis segments of aspherics," United States Patent Application 20060268282, filed May 2006, published October 2006.
[57] Dresel, Th.: "In situ determination of pixel mapping in interferometry," Intern. Application No. PCT/US2006/048419, (2006).
[58] Lowman, A. E. and Greivenkamp, J. E.: "Modeling an interferometer for non-null testing of aspheres," in *Optical Manufacturing and Testing*, V. J. Doherty and H. Stahl, eds., Proc. SPIE **2536,** 139–147 (1995).
[59] Pfund, J., Lindlein, N. and Schwider, J.: "Nonnull testing of rotationally symmetric aspheres: a systematic error assessment," Appl. Opt., **40**, 439-446 (2001).
[60] Schwider, J.: "Interferometric tests for aspherics," OSA TOPS, Vol. 24 Fabrication and Testing of Aspheres, (1999).
[61] Küchel, M.F., Sykora, D.M.: "Correlation Study between a New Interferometric Asphere Metrology System and Fizeau Interferometer," Key Engineering Materials, TRANS TECH PUBLICATIONS, (2008).